Noise Spectroscopy of Polymer Field Effect Transistors

A Thesis submitted in partial fulfillment
for the degree of
Master of Science (Engineering)

by

Rishav Harsh

Chemistry and Physics of Materials Unit
Jawaharlal Nehru Centre for Advanced Scientific Research
Bangalore – 560 064, India

SEPTEMBER 2015

Dedicated to Carl Sagan

DECLARATION

I hereby declare that the matter embodied in the thesis entitled **"Noise Spectroscopy of Polymer Field Effect Transistors"** is the result of investigations carried out by me at the Molecular Electronics Laboratory, Jawaharlal Nehru Centre for Advanced Scientific Research, Bangalore, India under the supervision of Prof. K. S. Narayan and it has not been submitted elsewhere for the award of any degree or diploma.

In keeping with the general practice in reporting scientific observations, due acknowledgment has been made whenever the work described is based on the findings of other investigators.

Rishav Harsh

CERTIFICATE

I hereby certify that the matter embodied in this thesis entitled **"Noise Spectroscopy of Polymer Field Effect Transistors"** has been carried out by Mr. Rishav Harsh at the Molecular Electronics Laboratory, Jawaharlal Nehru Centre for Advanced Scientific Research, Bangalore, India under my supervision and it has not been submitted elsewhere for the award of any degree or diploma.

Prof. K. S. Narayan

(Research Supervisor)

Acknowledgements

Incubation of an idea starts from an individual but its physical realization is a strongly correlated phenomena, especially in research. This page on acknowledgements is the outcome of contributions from many people, for the research work presented in this thesis.

Most significant and the major effort has been that of my teacher and guide, Prof. K. S. Narayan whose motivation, guidance, support, and patience has resulted in this document. I sincerely believe that it is not possible to appreciate his contribution in words, and can only say that learning from him has been a humbling experience and that his teachings will guide me throughout my life.

I thank my teachers and faculty members of JNC, Prof. Shobhana Narasimhan, Dr. N.S.Vidhyadhiraja, Prof. Chandrabhas Narayan, Prof. Umesh V. Waghmare, Prof. A.Sunderasan, Prof. Rajesh Ganpathy for course work, scientific discussions and doubt clearance sessions. I am very grateful to my course work teachers at IISc, Dr. Abhishek Singh , Prof. Navakanta Bhat, Prof. K. N. Bhat, Prof. S. A. Shivashankar and Prof. Srinivasan Raghavan.

I will be forever thankful to my labmates, Dr. Satyaprasad, Dr. Ravi, Dr. Murthy, Dr. Vini, Ashar, Prashant, Swathi, Raaghesh, Dhruv and Vikas who taught me the basics of experimentation (specially device fabrication), helped me with all the troubleshootings, and for maintaining a healthy, co-operative and scientific atmosphere in lab. Special thanks to Mr. Shashi (workshop) for tremendously helping me with the construction of faraday cage.

I thank the hostel wardens, Dr. Subi J. George and Dr. Sheeba Vasu, student representatives, hostel office and Dhanvantari staff for taking care of all the problems outside lab and within the campus. I sincerely thank JNC for the financial

support during this period. The staffs in Administration, Academic, Library, Accounts, and Complab for their timely support and help. I thank the garden staffs for maintaining this beautiful campus.

I thank my friends from NVSH, Aparna, Yamini, Krishnendu, Anand, Manjeet, Achal, Rafi, Shubhojit, Veena, Nikita, Surbhi, Pawan and Siddharth with whom I started my research carrier; friends in students residence Aishwarya, Shrilaxmi, Vikash, Sarika, Vybhav, Bhawani, Shantanu and Varun; from the JNC basketball club Divyesh, Ronak, Anudeep, Santosh, Aditya and Anupam; friends in IISc Nagarjun, Vikash, Saloni and Tribhuwan; friends from book club and movie club. These people are pillars of my social life in JNC and have made my stay a wonderful and memorable experience.

I am forever indebted to my parents and relatives for their support, encouragement, love and faith in me all these years. Last but not the least, special thanks to my laptop and LaTeXfor being instrumental in the preparation of this document.

Synopsis

Organic semiconductors have found a wide variety of application owing to a unique set of properties which facilitates large area fabrication and low temperature solution processing. The charge transport in these disordered material is modelled using gaussian distribution of states for site energy and position. Theoretical modelling in this case becomes complex due to lack of a periodic potential. Noise spectroscopy is being used here, as an alternative approach, to study the transport properties of organic semiconductors in a field effect transistor architecture. Low frequency noise analysis has been used extensively for silicon MOSFETs to calculate density of traps and/or defects at interface or in the dielectric, to address degradation issues, and used as a reliability tool. Noise in organic or polymer field effect transistors (OFETs or PFETs) have been studied with silicon and/or hafnium oxide as gate dielectric and the noise source has been attributed to traps in dielectric and at interface. In present study, noise analysis has been done on solution processable polymer dielectric and semiconductor based OFETs. Apart from gaining insight into charge transport of organic semiconductors, the study also becomes relevant in the context of using organic semiconductors for low cost flexible electronics.

The **first** part of thesis deals with experimental techniques comprising of device fabrication and noise measurement details of OFETs. The experimental setup for successfully extracting low frequency noise from the device under test (DUT) is carefully designed to eliminate noise from unwanted sources. Details of setup design is followed by the digital signal processing of sampled current from DUT. The main components for obtaining the frequency response or the power spectral density (PSD), comprises of DC batteries (for biasing), a trans-impedance preamplifier (for amplification of current signal) and a signal analyser to record the time series signal. Further processing is done on a desktop PC. Statistical averaging is done, giving sufficient time, to obtain accurate frequency response in the relevant range of frequencies.

The **second** part forms the most important as well as the largest portion of the thesis, dealing with noise studies in OFETs in different regimes and working modes. This part mainly consists of **four** types of noise measurements on n-type and p-type transistors. *First* study deals with the dependence of noise with drain-source

voltage keeping gate-source voltage constant, while the transistor is ON and under dark conditions, at room temperature.

The *second* study focuses on noise as a function of gate-source voltage keeping drain-source voltage constant, under similar conditions. The current noise is studied in linear and saturation regimes. The DC characteristics of OFETs have been explained by the equations developed for silicon MOSFETs. The noise modelling for the first two study is based on standard models developed for Si-MOSFETs as well. However, deviations are seen while applying these models, namely the mobility fluctuation model or the Hooge model and the carrier number fluctuation model or McWhorter model. From the PSD plots of the first two studies, it is observed that the origin of noise is a two dimensional (surface) phenomena which is expected since the conducting channel of transistor is formed at dielectric-semiconductor interface. The experimental fitting for obtained noise at high drain bias suggests mobility fluctuation. On the other hand the data fits more to McWhorter model (at low drain bias) however the fundamental assumption of underlying mechanism for conductivity fluctuation is not met here.

The *third* study investigates the noise properties of leakage gate current noise and its effect on the source-drain current noise, in a p-type transistor. High noise levels at gate terminal limits the frequency range of input waveforms and hence adversely affects the processing speed of circuits. The gate is the front end for input signals in most electronic circuits and thus it is quite important to study noise in this section of device, which has been scarcely attempted in polymer FETs. The spectral signature of gate current is seen at low frequency which dominates the source-drain current noise. In the PSD plot, gate noise component is identified by a higher exponent, on frequency term of the PSD equation, as compared to the source-drain noise.

The *fourth* and last study deals with light experiments on transistor operating in the depletion mode and compared with dark conditions, in similar bias conditions. The noise in this region is seen as a broad curve with a peak at around 1 kHz, spanning in a frequency range of 10 Hz to 10 kHz. This particular feature is usually associated with generation-recombination type noise with time constants having a distribution centered around the peak frequency. Upon the incident of light (green laser) at steady state, the noise amplitude as a whole increases, in the observed frequency range, retaining the shape of curve which corresponds to dark condition. The source of noise in depletion mode is attributed to bulk conductivity fluctuations in the semiconductor.

This thesis is an attempt to understand the charge transport properties of organic materials and address issues related to device stability and performance, by studying the noise or current fluctuations.

Publication

- *Noise spectroscopy of polymer transistors*, **Rishav Harsh** and K. S. Narayan

  (Manuscript under review)(2015)

Contents

Acknowledgements **vii**

Synopsis **ix**

Publication **x**

List of Figures **xiii**

Abbreviations **xviii**

Notations **xx**

1 Introduction **1**

1.1 Organic Semiconductors 2
1.2 Charge transport 3
1.3 Organic field effect transistor 8
1.4 Conductivity fluctuations 11
1.5 1/f-type noise 13
1.6 Other types of noise 15
1.7 Analytical models for noise 17
1.7.1 Mobility Fluctuation model 17
1.7.2 Number Fluctuation model 20
1.7.3 $\Delta N - \Delta\mu$ model 22
1.8 Noise in disordered semiconductors 23
1.9 Degradation and noise in OFETs 24
1.10 Outlook and Thesis Outline 25

2 Materials and Methods **27**

2.1 Materials 27
2.1.1 Dielectric Materials 27
2.1.2 Organic Semiconductors 28
2.2 Device Fabrication 29
2.3 DC Characterisation 30
2.4 Noise Setup 31

2.4.1 Sources of Noise 31
2.4.2 Noise Reduction 33
2.5 Instrument Configuration 34
2.5.1 Transimpedance amplifier (TIA) 34
2.5.2 Dynamic Signal Analyser (DSA) 36
2.6 Noise measurement 39

3 Noise Studies **41**
3.1 Experiments and measurements 41
3.1.1 BCB-N2200 transistors 42
3.1.2 BCB-P3HT transistors 44
3.1.3 PVDF-P3HT transistors 47
3.1.4 Leakage gate current noise 59
3.1.5 Effect of light 62
3.2 Discussions 64
3.3 Summary 71

Appendices **73**

A Matlab Code **75**

Bibliography **79**

List of Figures

1.1 Device architecture of field effect transistors 9

1.2 Schematic diagram showing operating regimes in a field effect transistor. The magnitude of gate bias is greater than the threshold voltage for all three cases. 10

1.3 (a). Time series plot of current fluctuations measured for 50 ohm resistor, (b). Gaussian curve fit to the current amplitude distribution (number of counts) for the time series data (in fig.(a)), (c). Power spectrum density as a function of frequency for the time series data (fig.(a)), and (d). Histogram plot of the time series data (in fig.(a)). The y-axis for fig.(a) and (b) has similar range and values, and plotted together for visual aid. 12

2.1 Schematic diagram showing steps of device fabrication 30

2.2 Power spectrum of channel noise at different levels of input range. . . 36

2.3 Schematic of the circuit for transistor noise measurement. 39

3.1 Source-drain current plotted as a function of gate bias (transfer curve) at different drain bias (V_{ds}), for n-type BCB-N2200 (BN) transistor before (fig-(a))and after (fig-(b)) the noise measurement. 42

3.2 Source-drain current plotted as a function of drain bias (output curve) at different gate bias (V_{gs}), for n-type BCB-N2200 transistor in fig-3.1. Channel length, L = 60 microns and width W= 0.91 mm. 42

3.3 Current noise spectrum of a BCB-N2200 transistor plotted as a function of frequency, at different gate bias. A reference 1/f-type plot with slope 1.5 is shown in dashed line. 43

3.4 Source-drain current plotted as a function of drain bias (output curve) at different gate bias (V_{gs}), for a p-type BCB-P3HT transistor. 45

3.5 Source-drain current plotted as a function of gate bias (transfer curve) at different drain bias (V_{ds}), for the p-type BCB-P3HT transistor in fig-3.4. Channel length, L = 50 microns and width W= 0.9 mm. . . . 45

3.6 Current noise spectrum of a BCB-P3HT transistor plotted as a function of frequency, at different drain bias. The gate bias is kept constant at $V_{gs} = -60V$. A reference $1/f^{\alpha}$ type plot with $\alpha = 1.5$ is shown in dashed line. 46
3.7 Source-drain current plotted as a function of drain bias (output curve) at different gate bias, for a p-type PVDF-P3HT (PP) transistor. The channel length $L = 30$ microns and channel width $W = 0.84$ mm. . . 48
3.8 Source-drain current plotted as a function of gate bias (transfer curve) at different drain bias, for the p-type PVDF-P3HT (PP) transistor in fig-3.7. 48
3.9 Square root (Y-axis right) and log scale (Y-axis left) plot of drain current v/s gate voltage (at $V_{ds} - 60V$) for a p-type PVDF-P3HT transistor (fig-3.7). The linear fit to the plot corresponding to $I_{ds}^{0.5}$ is shown in dashed lines which gives threshold voltage, V_{th} -15 V. . . . 49
3.10 Current noise spectrum ($S_I(f)$) plotted as a function of frequency, in linear regime at different drain voltage and constant V_{gs} (-60V) for a p-type PVDF-P3HT transistor (fig-3.7). The dashed line shows a reference 1/f plot. 50
3.11 Current noise spectrum ($S_I(f)$) plotted as a function of current magnitude for a p-type PVDF-P3HT transistor (fig-3.10). The transistor is operated in linear regime, gate voltage is at -60 V and drain voltage varied from -4 V to -24 V. The dashed lines show reference slope corresponding to current exponent β=1, in the Hooge relation. 50
3.12 Normalised power spectral density ($S(f)$) plotted as a function of frequency for a p-type PVDF-P3HT transistor. The transistor is operated in linear regime at different gate voltage and constant V_{ds} (-10V) The dashed line shows a reference 1/f plot. 51
3.13 Gate voltage dependence of relative noise spectrum ($S(f)$), at different frequencies, for a p-type PVDF-P3HT transistor operating in linear regime. The dashed lines show reference plot corresponding to $p = 2$. 52
3.14 Histogram plots for time series data for a p-type transistor operating in linear regime, obtained at different gate bias and constant drain bias (-10V). 53
3.15 Gaussian fitting of the histogram plots (fig-3.14) obtained at different gate bias for a p-type transistor, operating in linear regime. 54
3.16 Current noise spectrum ($S_I(f)$) plotted as a function of frequency, in saturation regime, at different gate bias and constant drain bias (-50 V) for a p-type PVDF-P3HT transistor (fig-3.7). The dashed line shows a reference 1/f plot. 55
3.17 Gate bias dependence of power spectrum (fig-3.16), in saturation regime, for a p-type PVDF-P3HT transistor. The dashed lines show reference plots corresponding to p =3 56

3.18 Source-drain current dependence of power spectrum (fig-3.16), in saturation regime, for a p-type PVDF-P3HT transistor. The dashed lines show reference plots corresponding to β =1.5 56
3.19 Histogram plots for time series data for a p-type transistor operating in saturation regime, obtained at different gate bias and a constant V_{ds} (-50V). 57
3.20 Gaussian fitting of the histogram plots (fig-3.19) obtained at different gate bias for a p-type transistor operating in saturation regime. . . . 58
3.21 Comparison between gate and source-drain current noise at a constant gate bias (-50V) for a p-type transistor (PVDF-P3HT). Reference $1/f^{\alpha}$ slopes are shown for α =1 and 2, in dashed lines. 59
3.22 Current noise spectra of gate and source-drain current shown for a high leakage p-type transistor (PVDF-P3HT), at constant gate bias ($V_{gs} = -50V$). Reference $1/f^{\alpha}$ slopes are shown for α =1 and 3, in dashed lines. 60
3.23 Frequency exponent, α (from Hooge relation), in the noise spectra of gate and channel current is plotted as a function of leakage current percentage ($C.P.$), for three devices-L1, L2 and L3 (p-type transistors based on PVDF-P3HT). Square shaped data points denote gate-exponent (α_g) while circles represent channel exponent α_{ch}. . . . 61
3.24 Noise spectrum of source-drain current for a p-type (PVDF-P3HT) transistor operated in accumulation and depletion mode, at constant V_{ds} (-50V). The dashed line shows reference 1/f slope. 62
3.25 Current noise spectrum in dark and light conditions for a p-type transistor (PVDF-P3HT) operated in depletion mode for $V_{gs} = 30V$ and $V_{ds} = -50V$ 63

Abbreviations

OSC	Organic semiconductor
OFET/PFET	Organic/polymer field effect transistor
LED	Light emitting diode
SD	Source-Drain
PSD	Power spectral (spectrum) density
RPSD	Relative power spectral (spectrum) density
HOMO	Highest occupied molecular orbital
LUMO	Lowest unoccupied molecular orbital
DOS	Density of states
FWHM	Full width at half maxima
DSA	Dynamic signal analyser
TIA	Trans-impedance amplifier
DUT	Device under test
g-r	generation-recombination
C.P.	Current Percentage

Notations

k_B	Boltzmann Constant (JK^{-1})
T	absolute temperature (K)
q	electronic charge (C)
f	frequency (Hz)
n	charge carrier density (cm^{-3})
μ	mobility ($cm^2V^{-1}s^{-1}$)
σ	conductivity (Scm^{-1})
I_{ds}	source-drain current (A)
V_{ds}	drain-source voltage (V)
V_{gs}	gate-source voltage (V)
C_i	Gate insulator/dielectric capacitance (Fcm^{-2})
L	Channel length (μm)
W	Channel width (mm)
$S_I(f)$	Current power spectrum density (A^2Hz^{-1})
$S(f)$	Normalised/relative power spectrum density (Hz^{-1})
γ_H	Hooge's constant

Chapter 1

Introduction

Practical demonstration of a working transistor by John Bardeen, Walter Brattain, and William Shockley in 1947 laid the foundation of electronics industry, and were awarded the Nobel prize in Physics (1956)[1] for the same. The electronic circuits that used vacuum tubes and triodes were supplanted by silicon based devices with the added advantage of reduced power consumption, smaller size, improved performance, large scale production, etc. Silicon based logic circuits find critical application in the field of computing, communications, space technology, manufacturing industries, aviation, defence, research, consumer electronics and many more. At present, all forms of technological advancements rely heavily on electronics.

The transistor is the functional building block of an electronic circuit. It has evolved through various stages, to meet varied requirements. It evolved from bipolar junction transistor(BJT) to junction field effect transistor(JFET) and later to metal-oxide-semiconductor field effect transistor (MOSFET). MOSFETs have gained popularity in complementary metal oxide semiconductor (CMOS) technology for making integrated circuits (ICs).[2] The word complementary refers to the fact that both p-type (holes as majority charge carriers) and n-type (electrons as majority charge carriers) MOSFETs are used, in a pair, for implementing logic functions. CMOS technology is used in microprocessors, microcontrollers, static RAM and various other digital logic circuits. The idea of ICs started with the development of small scale integration (SSI) devices comprising of few hundred transistors and finally achieved very large scale integration (VLSI) with millions of transistors on a single chip. An Intel i7 processor, today, typically contains few million transistors per

square millimetre.[3] This drastically reduces the cost per chip. However, the wafer on which the ICs are fabricated is presently limited to a diameter of 12 inch[a]. The most commonly used semiconducting material for making transistors is silicon although germanium, gallium nitride, gallium arsenide, silicon carbide, etc. are also seen as potential candidates for certain specific applications. Ultrapure crystals (purity$>$ 99%) are used for making substrate wafers which require very high temperature ($\sim 1400^0C$) for processing, substantially increasing the production cost. Further, the substrate wafer can only be increased to a certain size in order to have low cost per chip with a sustainable market strategy.[4] Thus, it is quite difficult for the silicon based technology to meet certain applications which demand large area electronics along with the desired virtue of being low cost. A promising candidate for such specific requirements is hydrocarbon based conducting materials often termed as organic semiconductors.

1.1 Organic Semiconductors

Organic semiconductors (OSCs) are compounds made of carbon and hydrogen atoms with few other heteroatoms like sulphur, nitrogen and oxygen, and show properties similar to inorganic semiconductors.[5] In 1977, the first highly conducting polymer, polyacetylene (chemically doped) was discovered, which demonstrated the utility of polymers as conductors or semiconductors. Heeger, MacDiarmid, and Shirakawa were awarded the Nobel Prize in Chemistry (2000)[6] for the discovery of conductive polymers. Molecular crystals like naphthalene and anthracene were studied before the discovery of conjugated polymers.[7] The field of OSCs was influenced significantly when higher conductivities were obtained in π-conjugated polymers[b](a system where the carbon chain has alternating single and double bonds) by doping the polymer.[8] With tedious research in the field of OSC, for the past two decade, it has been shown that these materials can be successfully used in solar cell, field effect transistor (FET) and light emitting diode (LED) applications.[9] They are potential candidates for low cost, large area and flexible substrate applications.[10]

Organic semiconductors can be broadly classified into two categories: small

[a]ongoing research is in the direction to make wafers of diameter 18 inch

[b]conjugated polymers will be used interchangeably with organic semiconductors

molecules or oligomers (usually processed in vacuum) and polymers (usually processed by wet chemical techniques).[5] In each case, various materials have been designed over the years that transport holes or electrons, or both (ambipolar). The processing temperature for wet chemical techniques is low as compared to silicon technology, thus reducing the manufacturing cost for this technology.

Organic semiconductors belong to a class of disordered materials. They show semiconducting properties albeit the "semiconducting" nature is different as compared to their inorganic counterpart.[11] Organic molecular crystals are van der Waals bonded solids[12] and have considerably weaker intermolecular bonding as compared to covalently bonded semiconductors, like Si or GaAs. This greatly affects their mechanical properties and enables them to be deposited on flexible substrates without worrying about structural damage due to folds and bends. In case of polymers, the polymeric backbone or chain can be arranged, either in an amorphous spaghetti-like structure, or form ordered domains with amorphous regions at their boundaries. In each of these cases, crystal structure or the packing of polymer chains show significant anisotropy which results in a certain degree of disorder, having a strong influence on the electronic properties of the material and consequently on the operation of organic electronic devices.

1.2 Charge transport

The charge transport properties of OSCs are briefly summarized in this section. The energy states of molecules are centered around the lowest unoccupied molecular orbital (LUMO) level and highest occupied molecular orbital (HOMO) level unlike inorganic semiconductors which have well defined conduction and valence band levels. The electronic wavefunctions are weakly delocalized among neighbouring molecules.[5] The density of states (DOS) around HOMO and LUMO levels are described by a Gaussian distribution.[13,14] The gaussian energy spectrum $g(\epsilon)$ is expressed as,

$$g(\epsilon) = \frac{N_o}{\sigma_o\sqrt{2\pi}} exp\left(\frac{-\epsilon^2}{2\sigma_o^2}\right) \tag{1.1}$$

here, σ_o is the standard deviation (energy spread or width) of the DOS, N_o is the

density of randomly distributed localized states (also known as sites). The energy ϵ is measured relative to the center of the DOS. The broadening of the DOS (expressed by σ_o) is known to be influenced more by the randomness of intermolecular interactions rather than its magnitude. The weak van der waals force and the morphology of disordered materials results in a *positional disorder* which is also modelled by a gaussian distribution[c].

The charge transport in these materials occurs due to "incoherent" hopping of carriers (electrons or holes) via randomly distributed localised states. The hopping rate (ν_{ij}) for carrier transition from an occupied site i to an empty site j, separated by distance r_{ij}, is described by the MillerAbrahams expression[11,12] given by,

$$\nu_{ij} = \nu_0 exp\left(-\frac{2r_{ij}}{\alpha_r} - \frac{\epsilon_j - \epsilon_i + |\epsilon_i - \epsilon_j|}{2k_B T}\right) \tag{1.2}$$

α_r is the localization length of charge carriers ($\sim 10^{-8} cm$), ϵ_i and ϵ_j are the carrier energies on sites i and j, respectively, k_B is the Boltzman constant, and T is absolute temperature. The prefactor ν_0, is termed as attempt-to-escape frequency which depends on the interaction mechanism that causes transitions of charge carries. In the case of interaction with phonons, its value is usually assumed close to the phonon frequency $\nu_0 \approx 10^{12} s^{-1}$. A carrier at site i can hop to another site j with three possibilities-

- Hopping to another site having higher energy $i.e$, $\epsilon_j > \epsilon_i$, assisted by absorption of a phonon. This is a thermally assisted tunnelling process and thus depends on temperature.

- Hopping into another site with equal energy, $\epsilon_j = \epsilon_i$, which occurs by tunnelling and is independent of temperature.

- Hopping into another site which has lower energy, $\epsilon_j < \epsilon_i$, where the energy difference is being compensated by the release of a phonon. This process is temperature independent.

If spatial positions and energies of localized states can be considered independent from each other, this model is traditionally called the Gaussian Disorder Model

[c]similar to eqn.1.1 and having standard deviation Σ.

(GDM). If site energies are correlated with their spatial positions the model is traditionally called the Correlated Disorder Model (CDM).[8] The energy spectrum in the latter case can also be Gaussian.

Two kinds of disorder are usually distinguished- *Diagonal Disorder*, which reflects the fluctuations in site energies (i.e., the energies of the HOMO or LUMO levels of individual molecules or chain segments) within the material; and *Off-Diagonal Disorder*, which is related to fluctuations in the strength of interactions between adjacent molecules or chain segments.[5] Off-diagonal disorder results in a distribution of electronic couplings within the material that can generate conducting pathways through the material as well as dead-ends for the charges. In the case of flexible molecules/chains, a major contributor to diagonal disorder is conformational freedom, as it leads to a distribution of torsion angles between adjacent moieties.[15] In addition, diagonal disorder is induced by electrostatic/polarization effects from surrounding molecules which vary with fluctuations in local packing.[9] In theoretical simulations, energetic disorder is generally described via a Gaussian distribution of HOMO/LUMO level energies; in conjugated polymers, the corresponding standard deviations are generally found to be of the order of 50-100 meV.

In an organic electronic device, the charge carriers are either injected into the organic semiconductors from metal or conducting oxide electrodes in the case of FETs and LEDs, or generated within the materials in the case of solar cells via photon-induced charge separation at the interface between electron-donor and electron-acceptor components. The anisotropy of charge transport in OSCs points out that the efficiency of transport is intimately related to the relative positions of the interacting molecules, and hence to crystal packing. The performance of organic electronic devices, thus, critically depends on the efficiency with which charge carriers (electrons and/or holes) move within the π-conjugated materials, or the conductivity of the material.

Conductivity

On a macroscopic level, the current density (J) through a material is given by the charge carrier density (n) and the carrier drift velocity (v_d), where the latter can be expressed by the mobility μ and the applied electric field F. We have $J = qn\mu F$

where the conductivity, σ is defined as

$$\sigma = qn\mu$$

Correlated in the conductivity equation, along with mobility, is charge carrier density. The density of injected carriers as well as mobility, is influenced by the strength of applied electric field.[16] At lower densities, all the carriers can be affected by trapping due to energetic disorder and/or impurities whereas at higher carrier densities, only a portion of the carriers are necessary to fill all the traps and the remaining carriers can experience trap-free transport.[17] However, it is possible that the filled traps, if charged, can increase scattering and lead to observed mobility values lower than the intrinsic values. Thus, both the density and mobility of charge carriers are influenced by nature and distribution of traps present in the material.[18]

It is observed that mobility in organic solids show an electric-field dependence. It is different in the case of single crystals and disordered materials. In single crystals, a field dependence is observed only in ultrapure crystals along the directions giving rise to the highest charge mobilities. In such instances, an increase in electric field is seen to reduce mobility. In disordered materials, an increase in mobility is observed at high fields.[9] The field dependence in the range $10^4 - 10^6$ V/cm generally obeys a Poole-Frenkel behavior,

$$\mu(F) \propto exp(\gamma F^{1/2})$$

where γ is temperature dependent. The experimental data is fit to the expression for γ given by,

$$\gamma = B\left[\frac{1}{k_B T} - \frac{1}{k_B T_0}\right]$$

here B is a constant and characteristic of the system, and T_0 is generally much larger than room temperature. However, a time of flight study on P3HT chains has led to T_0=250 K,[5,8,18] which implies that γ becomes negative above T_0 and the mobility decreases with increasing electric field. An understanding of this evolution can be found in the Bassler model[13] when off-diagonal disorder dominates diagonal disorder. Conceptually, this reflects the fact that, at low fields, the charges manage to follow the best percolation pathways and to avoid structural defects; higher

electric fields impose a stronger directionality and prevent the charges from moving around the defects, thereby reducing mobility.

Another factor that influences mobility is the presence of (chemical) impurities in the sample. Compounds that have a slightly different chemical structure than the compound under investigation, appear as side products of the chemical synthesis, are known to be present and usually classified as intrinsic impurities. A major impact on the transport properties can be expected when HOMO/LUMO levels of the impurities have energies that fall within the HOMO-LUMO gaps of the pure molecules.[18] In such conditions, a distinction is made between deep trap states (when the trapping energy is much larger than $k_B T$) and shallow traps (when the trapping energy is on the order of $k_B T$, which allows for thermal detrapping). In many instances, the exact nature of impurities/traps is difficult to determine.

The temperature dependence is markedly different in single crystals and in disordered materials.[8] In single crystals, the hole and electron mobilities generally decrease with temperature according to a power law evolution: $\mu \propto T^{-m}$. This decrease in mobility with temperature is typical of band transport and originates from enhanced scattering processes by lattice phonons, like metals. Depending on the degree of order, the charge carrier transport mechanism in organic semiconductors can fall between two extreme cases: *band* or *hopping transport*. Band transport is typically observed in highly purified molecular crystals at low temperatures. In highly disordered systems, transport generally proceeds via hopping and is thermally activated.[11] Higher temperatures improve transport by providing the energy required to overcome the barriers created by energetic disorder. The temperature dependence has been often fitted to an Arrhenius-like law:

$$\mu \propto exp(-\Delta/k_B T)$$

where Δ is the activation energy and increases with the amount of disorder. Thus, charge transport in OSC is dictated by several intrinsic and extrinsic parameters, which are often convoluted among each other.

It is clear that conductivity in organic solids depends on various factors and is mostly influenced by the chemical purity and the structural order present. Even inorganic semiconductors are influenced by the presence of defects, impurities and

the lattice vibrations.

The physical and chemical properties of OSC can be tuned or altered by effective design strategies. For instance, the side alkyl chain in a polymer backbone is known to affect solubility and degree of crystallinity in thin films.[8] Similarly, a wide range of such functionalities like processing temperature, band gap, nature of charge transport (p-type or n-type), conductivity, etc can be influenced by careful molecular design and processing techniques.[9] These organic materials based on their design, structure and photophysics find applications in solar cell, field effect transistor and light emitting diode device architectures. They have already caught attention of some companies like Sumitomo, DuPont, Solvay, BASF, Ciba, PARC, Polyera, Merck, etc who are actively engaged in research and development of efficient organic materials as well as in their application.[19] In this thesis, conjugated polymers have been used in FET architecture to study the charge transport in the material as well as its device properties. The next section deals with the electrical transport in FETs.

1.3 Organic field effect transistor

Organic field effect transistors (OFETs)[(d)] have gained commercial importance for their application in cheap and flexible electronic circuits. Organic FET-based active matrix backplanes on plastic substrates are close to being commercialized in lightweight, robust, flexible displays for electronic reading applications.[19] OFET-driven liquid-crystal displays (LCD) and organic light-emitting diode (OLED) displays have already been demonstrated.[19] Impressive progress has also been made in realizing logic circuits based on OFETs for applications in radio frequency identification tagging (RFID) and chemical or biological sensing.[20]

The key quantity that characterizes charge transport, in an OFET, is the carrier mobility.[21] The focus is to design better and new molecules to achieve higher mobility values in an OFET. An OFET is similar to MOSFET in device architecture where the dielectric and semiconductor is replaced by an organic material. Both small molecules and conjugated polymers have been used as semiconductor in OFETs. The choice of material largely depends on charge carrier mobility and

[(d)] OFET will be used interchangeably with PFET, in this thesis

processing requirements. A schematic of device structure for a MOSFET and an OFET is shown in fig.1.1.

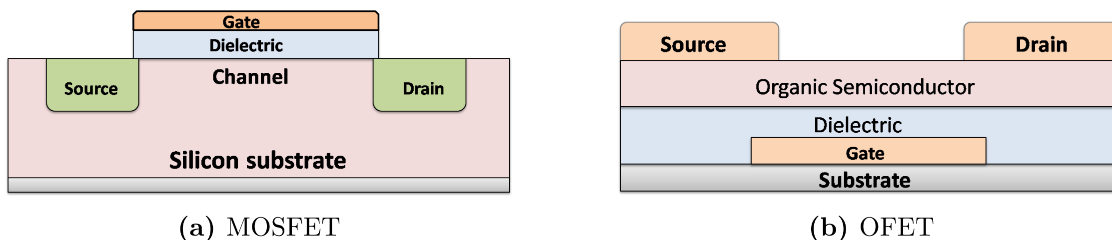

(a) MOSFET

(b) OFET

Figure 1.1: Device architecture of field effect transistors

Silicon MOSFETs are grown on a single crystal silicon wafer where the drain and source regions are formed by heavy doping with n-type or p-type elements, the dielectric is formed by the sacrificial oxidation of silicon to form silicon dioxide and is followed by metal deposition to form electrodes for source, drain and gate.[2] Other materials like hafnium oxide and aluminium oxide have also been explored, as dielectric, for better performance. Inorganic MOSFETs usually work in inversion region where the gate voltage creates an inversion region of minority charge carriers near the dielectric-semiconductor interface.

The device structure shown for OFET (fig.1.1b) is a bottom-gate top-contact (BGTC) architecture where the gate electrode is deposited on a clean substrate (like glass or polyethylene terephthalate) followed by thin film deposition of dielectric and semiconductor layers, and finally evaporation of metal to form source-drain contacts. Voltage bias is applied to the gate electrode (V_{gs}) and the drain electrode (V_{ds}), with respect to the source electrode kept at ground ($V_s = 0$). In case of OFETs, the transistor works in accumulation where the gate bias creates a charged region at the dielectric-semiconductor interface which is conducive for the transport of one type of charge carriers, through the semiconductor.[21] Molecules that readily give up electrons are well suited to transport holes and are thus referred to as hole-transporting molecules (p-type), while the converse is the case for electron-transporting or electron-accepting molecules (n-type). In a p-type OSC the gate bias is of negative polarity which creates a positively charged interface (accumulation) facilitating transport of holes through the channel. The device operation of OFETs

is established on the working of inorganic MOSFETs.

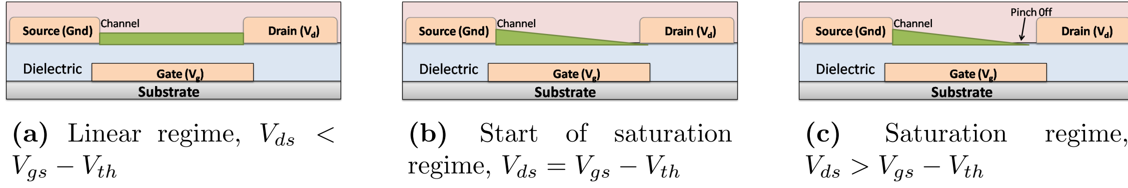

(a) Linear regime, $V_{ds} < V_{gs} - V_{th}$ **(b)** Start of saturation regime, $V_{ds} = V_{gs} - V_{th}$ **(c)** Saturation regime, $V_{ds} > V_{gs} - V_{th}$

Figure 1.2: Schematic diagram showing operating regimes in a field effect transistor. The magnitude of gate bias is greater than the threshold voltage for all three cases.

The basic operating regimes of FET are shown in figure 1.2.The gate bias (V_{gs}) is responsible for accumulation of charge carriers at the interface, however because of the distribution of localised energy states near HOMO and LUMO levels, a certain minimum threshold voltage (V_{th}) must be reached before the charge carriers are mobile and the entire channel becomes conducting.[22] The channel is formed in the transistor when the magnitude of gate voltage (V_{gs}) is greater than that of V_{th}. This situation is depicted in fig.1.2a where the channel has been formed and V_{ds} is much less than ($V_{gs} - V_{th}$), referred to as the linear regime where the current flowing through the channel, I_{ds} is directly proportional to V_{ds}. When V_{ds} is further increased, a point is reached when $V_{ds} = V_{gs} - V_{th}$ at which the channel is *pinched off* (fig.1.2b). Beyond this point, I_{ds} saturates (fig.1.2c) and increases only marginally with increasing V_{ds}.

The current-voltage characteristics can be described by assuming the gradual channel approximation (where the electric field due to V_{gs} is much larger than field due to V_{ds}). The current expression[22] is given by

$$I_{ds} = \frac{W}{L}\mu C_i \left[(V_{gs} - V_{th})V_{ds} - \frac{V_{ds}^2}{2}\right] \tag{1.3}$$

here,

W is channel width,

L is channel length,

μ is mobility, and

C_i is insulator/dielectric capacitance.

In linear regime, when $V_{ds} \ll V_{gs} - V_{th}$, one obtains

$$I_{ds} = \frac{W}{L}\mu_{lin}C_i(V_{gs} - V_{th})V_{ds} \tag{1.4}$$

and, at the onset of saturation regime ($V_{ds} = V_{gs} - V_{th}$), the channel current is approximated as

$$I_{ds,sat} = \frac{W}{2L}\mu_{sat}C_i(V_{gs} - V_{th})^2 \tag{1.5}$$

To obtain mobility in linear regime (μ_{lin}), we have from eqn.1.4

$$\mu_{lin} = \left(\frac{\partial I_{ds}}{\partial V_{gs}}\right)_{V_{ds}} \frac{L}{WC_i} \tag{1.6}$$

and can be calculated by obtaining the slope of transfer curve ($I_{ds} - V_{gs}$) at a given V_{ds}. Similarly, for saturation regime, the square root of I_{ds} goes linear with V_{gs}^{eff}[e](eqn.1.5) and the saturation mobility (μ_{sat}) can be extracted from the $\sqrt{I_{ds}}$ v/s V_{gs} plot.

1.4 Conductivity fluctuations

It has been observed that the instantaneous value of conductivity, in any sample, fluctuates around a mean value (σ). These fluctuations, observed in the time series of current or voltage signal, is termed as ***noise***.[23] In condensed matter, the fluctuations are related with measured conductivity of systems like bulk materials, thin films, nanowires, 2D materials, etc.[24] Noise has been observed in metallic crystals as well as organic solids. In the latter case, the fluctuations are more pronounced due to a lower carrier density and a host of other factors that influence the charge transport mechanism.

Noise has been observed in a multitude of systems ranging from physical, biological, chemical, astronomical, musical, physiological, climatic and various others. Current or voltage fluctuations in solids are typical random processes. It consists of frequency components that are random in amplitude and phase. A random process is a random function ($v(t)$) of an independent variable t which in this case is time. The random function $v(t)$ denotes the sampled voltage signal as a function of time. Random (voltage) signals typically occur due to many independent

[e]Effective gate voltage V_{gs}^{eff} is defined as, $V_{gs}^{eff} = V_{gs} - V_{th}$

contributions (from charge carriers) and they are mathematically described by a *stochastic* process. A random signal can have fluctuations around a mean *rms* value and is termed as *stationary* random signals where the mean value remains constant. However, over long sampling durations, most random signals are non-stationary. Random processes are usually described by their ***spectral*** characteristics (spectral density) or correlation function, and its ***amplitude*** characteristics, for example, the probability density function.

Time domain representation

The ***central limit theorem*** states that the distribution of the sum (or average) of a large number of independent, identically-distributed variables will be approximately normal (or a gaussian distribution), regardless of the underlying distribution.

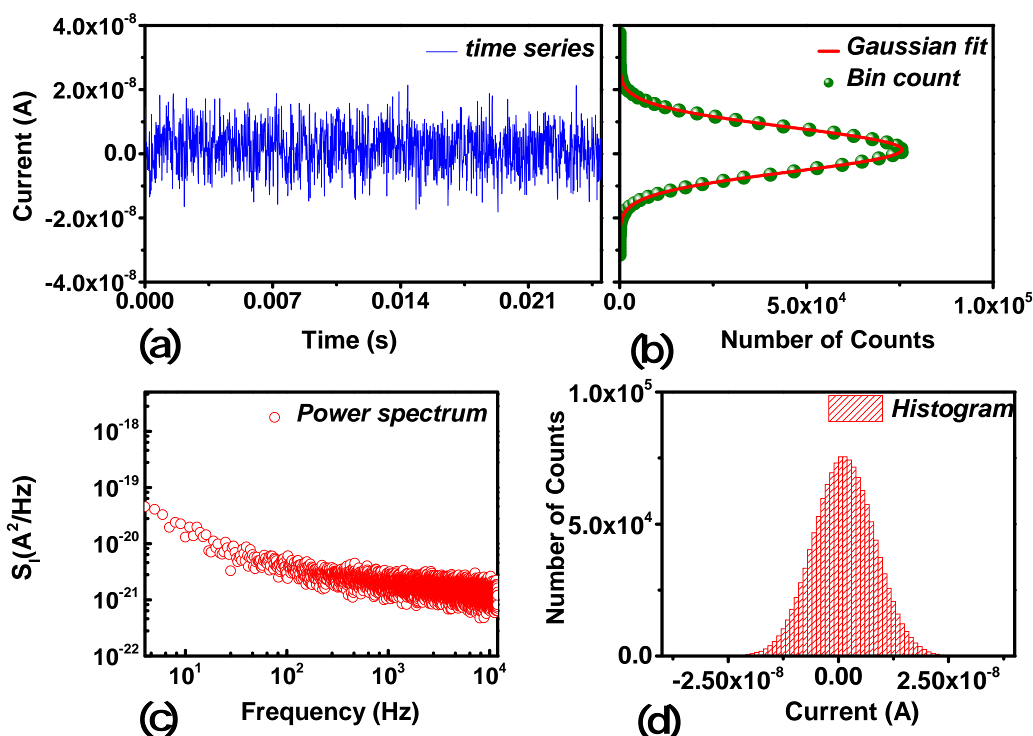

Figure 1.3: (a). Time series plot of current fluctuations measured for 50 ohm resistor, (b). Gaussian curve fit to the current amplitude distribution (number of counts) for the time series data (in fig.(a)), (c). Power spectrum density as a function of frequency for the time series data (fig.(a)), and (d). Histogram plot of the time series data (in fig.(a)). The y-axis for fig.(a) and (b) has similar range and values, and plotted together for visual aid.

Normal or **gaussian** distribution function has a "bell" shape curve and has been used in section-1.2 to characterise the DOS around the HOMO/LUMO levels. The sampled current signal, here, can be treated as a series of independent random events. The current output from OFETs is digitally recorded and stored as time series data. In time domain representation, this digital data is plotted as a function of time (fig-1.3(a)) or plotted as histogram (fig-1.3(d)). The amplitude distribution of current fluctuations for a (50 Ω) resistor has been observed to fit quite appropriately to a gaussian curve (fig.1.3). A gaussian distribution is defined by two parameters, the mean (x_i) and the standard deviation (σ_i) or full-width at half maxima (FWHM)[(f)]

Frequency domain representation

For frequency domain analysis, noise in a signal is expressed in terms of root mean square (*rms*) value of the amplitude of the observed quantity (voltage, current, etc.). Frequency response of the signal (time series data) is obtained by taking the fourier transform[(g)] of the sampled data. The magnitude of fourier transform gives amplitude spectral density ($V/\sqrt{Hz}$ or $A/\sqrt{Hz}$) while the square of the magnitude gives the power spectral density (V^2/Hz or A^2/Hz). The sampled voltage signal is normalized by the transimpedance gain to obtain current power spectrum density ($S_I(f)$). The current power spectrum for the resistor is shown in fig-1.3(c).

1.5 1/f-type noise

Noise in electronic systems is an important field of investigation because its presence limits device performance and is a bottleneck for practical applications.[23,25–27] Numerous factors can contribute to the total noise present in an electronic device.[28–30] The sources can be broadly classified into two groups-

1. Intrinsic material property which influences the charge transport mechanism like the lattice structure, the presence of defects/impurities, and charge carrier

[(f)] $FWHM \approx 2.35\sigma_i$

[(g)] *fast fourier transform*, since the data length is finite and is digital.

density. The noise in this case is intrinsic or *fundamental* in nature, for a given material.

2. Processing and fabrication related noise sources that includes growth and/or deposition of dielectrics, thin films, metal contacts, the interfaces, etc. These sources are *extrinsic* in nature, and can be minimized by careful design and processing techniques.

In general, fluctuations in the current signal result from the different arrival times of charge carriers at the collecting electrodes. The free charge carriers traverse through an energetic landscape which has been modified by impuritties, defects, interface states and the disorder in the material itself (in case of OFETs), which subsequently affects the scattering and/or trapping-detrapping of the mobile charge carriers, and is observed as noise. Thus, the charge transport in the device is reflected in the noise of the signal.[25] In an attempt to identify mechanisms which contribute to noise in the source-drain current of the PFETs, noise has been studied in the low frequency regime in this thesis.

Appearing in all kinds of electronic devices and many other non-physical systems, noise typically has a 1/f type spectrum at low frequencies.[23] It has captured the attention of researchers from various disciplines. To a physicist, the noise in an electronic system represents a manifestation of some physical phenomena that can be described by statistical mechanics and an understanding of its practical consequences helps clarify some concepts of the physical theory. To an electronics engineer, noise is a constraint of the real systems but a better understanding of its physical origins helps them to minimize its effects and design instruments with improved performance. For example, low-frequency noise is one of the main problems in designing a low-noise amplifier, used for very sensitive applications. It becomes more crucial in modern integrated circuit engineering, as the device size continues to shrink and more MOS devices are used in analog circuits. It dominates in the power spectrum of metals, semiconductors, and a variety of other materials. The generality of 1/f-type noise has sparked a lot of interest among researchers and is currently investigated in organic field effect transistors.

The power spectrum S_f shows $1/f^{\alpha}$ dependence, with α in the range of 0.8 -1.4. For exponent values very close to unity, this excess noise is known as $1/f$ noise[h] , else it is referred to as $1/f$-type noise.

1.6 Other types of noise

Noise in solids have been studied for more than seven decades now. Different type of sources/systems show different frequency response and is briefly mentioned in this section.

Thermal Noise

Also known as Johnson or Nyquist noise, it arises in any resistor of resistance R at temperature T. The voltage power spectral density (V^2/Hz) is given by

$$S_V(f) = 4k_BTR \tag{1.7}$$

similarly, the current power spectral density (PSD) (A^2/Hz) is given by,

$$S_I(f) = 4k_BT/R \tag{1.8}$$

Thermal noise is independent of frequency, thus having a white noise spectrum and exists in almost all kinds of electronic systems.. The spectral power is independent of the current flowing through the resistor. Johnson noise doesn't distinguish between material as long as the resistance value is the same.

Shot Noise

The shot noise arises from current flowing in a conductor and is also white in nature. The spectral power is given as $S_I(f) = 2qI$ where q is the electronic charge and I represents the current. In general, the shot noise is observed at low temperatures when the thermal noise does not dominate.

[h]also known as *pink* or *flicker* noise

Generation-recombination (g-r) Noise

Generation-recombination (g-r) noise in semiconductors originates from traps that randomly capture and emit carriers, thereby causing fluctuations in the number of carriers available for current transport. In semiconductors, electronic states within the forbidden bandgap are referred to as traps, and exist due to the presence of various defects or impurities in the bulk and at its surface.[?] With a free charge carrier density N, the PSD of number fluctuation[31] is given by

$$S_N(f) = 4\overline{(\Delta N)^2}\frac{\tau}{1+(2\pi f\tau)^2} \tag{1.9}$$

where τ is the time constant for the transitions. The shape of the spectrum given by equation 1.9 is called a Lorentzian spectrum.

Random Telegraph Signal (RTS) Noise

A special case of g-r noise is the random telegraph noise (burst or popcorn noise), which is viewed as discrete switching events in the time domain. The waveform resembles a square pulse of randomly varying duty cycle and pulse width, similar to a random telegraph message. The two levels remain constant and switching is random, the PSD for the RTS noise and the g-r noise are both of the Lorentzian type. In fact, g-r noise can be viewed as a sum of RTS noise processes from one or more traps with identical time constants, and is only displayed as RTS noise in the time domain if the number of traps involved is small. RTS noise is an interesting phenomenon since the random switching process from just one trap can be studied in the time domain. It is established that RTS noise is caused by a single carrier controlling the flow of a large number of carriers rather than a large number of carriers being involved in the trapping/detrapping process, thus a single electron can be studied.

The frequency response or the noise spectrum provides information about the nature of electronic transitions that are present in a material. Usually these transitions are recorded in the form of fluctuating voltage or current signal. More accurately these are conductivity fluctuations and is dealt in the next section.

1.7 Analytical models for noise

Current or conductivity fluctuations ($\Delta\sigma = \Delta(qn\mu)$) are related to the fluctuation in charge carrier density (ΔN model or McWhorter model) or mobility fluctuation ($\Delta\mu$ model or Hooge model) or sometimes both.[32–34] These models have been extensively applied to study noise in FETs,[26] and other systems as well. In this section, a very brief description of these theories is presented.

Flicker noise in thin film transistors (TFTs) can be analysed according to McWhorter's or Hooge's theories, as has been done for crystalline Si MOSFETs.[35,36] In the former case, the 1/f noise is attributed to carrier number fluctuations (ΔN model) due to the random trapping and detrapping of charges from the traps located near the dielectric-channel interface. While the latter is concerned with the bulk mobility fluctuations ($\Delta\mu$ model) due to scattering of charge carriers. A trapping noise model with correlated mobility fluctuations (ΔN-$\Delta\mu$ model) can also be taken into account to describe possible effects of dielectric charge fluctuations on carrier mobility.[37] A brief description of these models are mentioned in subsequent sections.

1.7.1 Mobility Fluctuation model

The most celebrated empirical relation for analysing noise is the *Hooge's* relation for power spectral density (PSD) which was first proposed for equilibrium resistance fluctuations in homogenous samples and gradually applied to other systems, for its simplicity.[27] Hooge gave this relation based on the assumption that noise arises from the bulk of the solid and that it results from lattice scattering of charge carriers.[28] The spectral power in observed resistance fluctuations is given as,

$$\frac{S_R(f)}{R^2} = \frac{\gamma_H}{Nf} \tag{1.10}$$

For homogeneous ohmic samples, where the relation between current and voltage is linear, Hooge relation can also be expressed as

$$\frac{S_R(f)}{R^2} = \frac{S_V(f)}{V^2} = \frac{S_I(f)}{I^2} = \frac{\gamma_H}{Nf} \tag{1.11}$$

where $S_R(f)$ is the resistance PSD (Ω^2/Hz), γ_H is Hooge's constant (material property), N is the total number of charge carriers and f frequency (Hz). The

fundamental assumption is that the resistivity fluctuations (or noise) arises from the independent motion of N electrons (charge carrier) i.e. whatever the electrons do to produce the 1/f spectrum, they do it independently.[23] The Hooge's constant γ_H, earlier thought of as a universal constant (2×10^{-3}) for materials, has been shown to depend on the purity of the material.[38] The central idea behind the use of 1/f noise is based on the fact that noise is a resistance (or conductivity) fluctuation and that it has a defect origin, which has been experimentally established on metal films and semiconductors.[39] However, it gives a good estimate of the relative noise present in a system, and is useful for comparisons. The noise in a solid depends on its quality and purity which makes noise spectroscopy a valuable tool[31] in materials characterization.

To study noise properties of some external parameter (current, temperature, light, doping, etc.), the magnitude of 1/f noise has to be well above the thermal noise level ($4k_BTR$). Thus, the joule heating of the sample should be avoided by passing high currents which sets a limit to N and, as an approximation N should be less than 10^{13}. This means that for a observable 1/f noise, metal samples should be smaller than 10^3 μm^3 and semiconductor samples (with free charge carrier density, n $\approx 10^{17}$ cm^{-3}) could be much larger, upto 1 mm^3. The reverse is also true, to make samples free of 1/f noise the samples should be made larger than the given dimensions.[35]

In ohmic (or linear) operation of transistors, the total number of free carriers (N) can be estimated from the following relations;

$I_{ds} = \frac{qN}{t} = \frac{qN}{L/v_d} = \frac{qNv_d}{L}$

while, drift velocity, $v_d = \frac{\mu V_{ds}}{L}$ which gives,

$$N = \frac{L^2 I_{ds}}{q\mu V_{ds}} = \frac{L^2}{q\mu R_{ch}} \tag{1.12}$$

"N' can also be calculated from the gate bias from the following relation

$$N = C_i W L(V_{gs} - V_{th}) \tag{1.13}$$

In the linear regime, the two equations (eqn.1.13 and 1.12) are similar. The PSD in this case can be written as,

$$S_I(f) = \left(\frac{q\gamma_h}{WLC_i}\right)\frac{I_{ds}^2}{(V_{gs}-V_{th})}\frac{1}{f} \tag{1.14}$$

Using eqn.1.5 and 1.14, the PSD for saturation regime can be written as,

$$S_I(f) \propto \frac{I_{ds}^2}{(V_{gs}-V_{th})}\frac{1}{f} \propto (V_{gs}-V_{th})^3\frac{1}{f} \tag{1.15}$$

The current noise spectra is usually analysed by Hooge's empirical relation, and is expressed as,

$$S_I(f) = \frac{\gamma_H I^2}{Nf} \tag{1.16}$$

Another way of representing above equation (eqn.1.16) is in terms of relative or normalised power spectral density (RPSD), obtained by normalising the power spectral density by the square of current magnitude.

$$S(f) = \frac{S_I(f)}{I^2} = \gamma_H/Nf \tag{1.17}$$

Relative or normalised PSD shows an inverse dependence with the number of charge carriers N, implying that noise amplitude is more pronounced when charge carriers are less, and vice versa. A more useful and modified form of Hooge's expression is

$$S_I(f) = \gamma_H I^\beta/Nf^\alpha \tag{1.18}$$

Hooge's equation, originally developed for metals, has been applied to a variety of electronic systems.[24] The exponents on current bias (β) and frequency (α) deviate from the proposed value of 2 and 1, respectively, for many systems. These exponents are obtained by experimental fitting to observed PSD plots. The β value is a measure of the mixing of various noise sources in the device[40] and to distinguish between the volume versus surface (interface) origin of noise source.[30,41] For surface trapping $\beta \sim 1$ and for volume trapping $\beta \sim 1.5-2$. The α value is interpreted as a measure of the distribution of traps responsible for the carrier number fluctuations. A value close to unity (± 0.2) is indicative of uniform distribution of trap energies. However, Hooge's mobility fluctuation model is applied only when the observed

flicker noise has α equal to or very close to unity, any deviation from such behaviour is not explained in this framework since γ_H becomes frequency dependent and the frequency has to be specified for obtaining hooge's constant (which should ideally be independent of frequency). The modified expression for PSD (eqn.1.18) is being used in subsequent sections, to analyse the spectral features.

1.7.2 Number Fluctuation model

In the number fluctuation model or the McWhorter model, the 1/f noise is due to generationrecombination (g-r) noise resulting from electron transitions between the conduction band of the channel material and the traps in the oxide layer of the metal-oxide-semiconductor transistor. This model has been very successful, particularly for the n-channel transistors where it is assumed that the electron trapping-detrapping events occur between the gate oxide and the channel, through quantum tunneling. The basic assumption is that the trap states are homogeneously distributed along the distance (s) from the interface. The trapping time constant (τ) depends exponentially on distance s from the interface. It is given as $\tau_s = \tau_0 \exp(s/\lambda)$ where λ is the tunnelling parameter ($10^{-8} cm$) which gives the relaxation function (statistical weight) $g(\tau)$,

$$g(\tau)d\tau = \left(\frac{1}{ln(\tau_h/\tau_l)}\right)\frac{d\tau}{\tau} \tag{1.19}$$

where the terms in bracket are used for normalising the integral when computing the power spectrum. The spectrum ($S(\tau)$) resulting from carriers trapping-detrapping at some distance s having time constant τ is obtained as a Lorentzian spectrum, given by

$$S(\tau) \propto \frac{\tau}{1 + (2\pi f \tau)^2} \tag{1.20}$$

The power spectrum thus can be obtained by the integration over time constants in a range that represents the smallest(τ_l) and largest distances(τ_h) . Thus we have,

$$S(f) \propto \int_{\tau_l}^{\tau_h} S(\tau)g(\tau)d\tau$$

$$\propto \int_{\tau_l}^{\tau_h} \frac{\tau}{1 + (2\pi f \tau)} \frac{1}{\tau} d\tau$$

or,

$$S(f) \propto \frac{[tan^{-1}(2\pi f\tau_h) - tan^{-1}(2\pi f\tau_l)]}{2\pi f} \tag{1.21}$$

Depending on the value of τ_l and τ_h, the power spectrum will have the following dependencies,

$$S(f) \propto \begin{cases} const. & \text{for } f \ll 1/\tau_l, \\ 1/f & \text{for } 1/\tau_l < f < 1/\tau_h, \\ 1/f^2 & \text{for } f \gg 1/\tau_h. \end{cases} \tag{1.22}$$

From equation 1.22, at very low frequency, the noise power becomes constant and the integral converges, unlike the Hooge relation. Thus, the Mcwhorter model is much preferred because of the benefit of having a mathematical treatment,[37] however, the underlying assumptions may not be always valid.

In McWhorter theory, the current noise spectral density, for silicon MOSFETs,[42] can be expressed as

$$S_I(f) = \left(\frac{k^*\mu}{fC_iL}\right)\frac{I_{ds}V_{ds}}{(V_{gs} - V_{th})} \tag{1.23}$$

In this expression, k^* takes into account the electron tunnelling from insulator traps near the interface to the conducting channel, and vice versa. This formulation works well with oxide based dielectrics (like SiO_2), and in that case

$$k^* = \frac{q^2 D_t(E_F)kT}{ln(\frac{\tau_h}{\tau_l})} \tag{1.24}$$

where, $D_t(E_F)$ is the active trap density in the vicinity of the Fermi level (E_F). In linear regime, eqn.1.23 can be modified using the I-V relation (eqn.1.4) to obtain,

$$S_I(f) = \left(\frac{k^*}{WLC_i^2}\right)\frac{I_{ds}^2}{(V_{gs} - V_{th})^2}\frac{1}{f} \tag{1.25}$$

or,

$$S_I(f) \propto \frac{I_{ds}^2}{(V_{gs} - V_{th})^2}\frac{1}{f}$$

And for saturation regime we obtain, using eqn.1.5

$$S_I(f) \propto \frac{I_{ds}^2}{(V_{gs} - V_{th})^2}\frac{1}{f} \propto (V_{gs} - V_{th})^2\frac{1}{f} \tag{1.26}$$

The interface-trap density(N_t) in Si-MOSFETs, in the sub-threshold conduction ($V_{gs} < V_{th}$), is evaluated from the relative current noise spectrum using the following relation,

$$S(f) = \frac{q^4 N_t}{\delta k_B T W L C_i^2} \left(\frac{1}{f}\right) \tag{1.27}$$

where, δ is the attenuation coefficient of the electron wave function. The value of tunnelling parameter or the tunnel penetration depth (λ), which is defined as $\lambda = 1/\delta$, is estimated to be 0.1 nm for $Si - SiO_2$ system.

1.7.3 $\Delta N - \Delta\mu$ model

The $\Delta N - \Delta\mu$ model[37,42,43] applies when the carrier number fluctuations induce noticeable changes in the mobility. The normalised drain current spectral density has been related to the voltage spectral density by the following relationship,

$$\frac{S_I(f)}{I^2} = \left[1 \pm \alpha_s \mu C_i \frac{I_{ds}}{g_m}\right]^2 \left(\frac{g_m}{I_{ds}}\right)^2 S_V(f) \tag{1.28}$$

here, α_s is a constant correlated with the sensitivity of the mobility to the interface charge coulomb scattering and $g_m \left(= \frac{\partial I_{ds}}{\partial V_{gs}}\right)$ is the device transconductance, where, $S_v(f)$ has been expressed as,

$$S_V(f) = \frac{q^2 k T N_t}{\delta W L C_i^2 f} \tag{1.29}$$

For pure ΔN model we have $\alpha_s = 0$ which gives,

$$\frac{S_I(f)}{I^2} = \left(\frac{g_m}{I_{ds}}\right)^2 S_V(f) = \left(\frac{g_m}{I_{ds}}\right)^2 \frac{q^2 k T N_t}{\delta W L C_i^2 f} \tag{1.30}$$

Eqn.1.30 has been used extensively for calculating trap density in MOSFETs (based on silicon, MoS_2, graphene, etc).[44,45] However, the calculation of N_t requires the value of tunnelling parameter (λ or δ) for the dielectric which is difficult to obtain for a polymer dielectric.

1.8 Noise in disordered semiconductors

Noise in homogenous crystalline solids, like metals and semiconductors, are mostly dominated by mobility fluctuations.[27,29,30] In case of disordered materials, like amorphous Silicon (a-Si) and organic semiconductors, the mobility and number density largely depend on the growth dynamics and/or processing conditions.[9] The presence of small range crystal domains and grain boundaries provide scope for both trapping-detrapping and scattering of charge carriers.[46] In these materials, low frequency noise is more pronounced at room temperature and generally takes a 1/f-type spectrum.

The origin of 1/f noise in solids has been the topic of active debate for nearly half a century.[24,47] There are two popular schools of thought, namely, the mobility fluctuation model (Hooge model) and the number fluctuation model (McWhorter model).[32–34] In hundreds of publications, there is ample support for any theory and many counterarguments against the alternative. As mentioned earlier (section-1.7), any submicron system has a 1/f noise (usually) and either of the models can be fitted to prove or disprove a certain model. There have been reports which confirm and deny the same model in a given system.

The common acceptable point is that the flicker noise may have different origins and properties. Similarities of spectra in different systems may be due to the similar mathematical processes, for example, in Mcwhorter model the 1/f noise is the summation of individual Lorentzians,[35] which can be the case for some other systems as well. In that case, the physical process that contributes to distribution of time constants and a Lorentzian spectrum might have different origin but the collective response over a given bandwidth may sum up to a 1/f type noise.[25] Despite a lot of effort dedicated towards the understanding of noise, its exact physical origins are still unclear in most systems and the disputes on the origin of 1/f noise are still unresolved so far. Several models of different origins have been proposed to interpret the observed 1/f noise in different electronic devices or experiments.[23] But they can applied to very specific situations considering idealistic assumptions. In most cases, the actual observed spectra are ordinarily of the form ($0.8 < \alpha < 1.4$) over a wide frequency range ($\sim 1Hz - 10kHz$) and has been used to correlate a change in some parameter (annealing conditions, surface treatment, film thickness, etc)[46,48–50] with

the noise amplitude (in a PSD plot). However, these observations become more complicated when various competing factors, each having 1/f type behaviour, are present and contribute to the total observed spectrum.

1.9 Degradation and noise in OFETs

The operational stability of OFETs is influenced by extrinsic factors, such as oxidation or presence of moisture, and intrinsic factors, such as the inherent structural and electronic disorder that is present in thin organic semiconductor films.[19,51] Some of the high-mobility organic semiconductors, such as pentacene and poly-3-hexylthiophene (P3HT), are known to suffer from chemical instabilities when exposed to atmospheric species, and light.[52] In some systems, device instabilities are more pronounced in humid atmosphere than in vacuum. There is clear evidence in many systems that hysteresis is due to the moisture uptake in the polar polymer dielectric. For many OFET materials and device structures, bias stress measurements have been reported which significantly affects the device performance. Device degradation commonly manifests itself as

- a shift of the threshold voltage,
- an increase in the sub-threshold slope,
- a reduction of the field-effect mobility,
- an increase of the OFF current, and/or
- increased hysteresis between subsequent measurements in transistor characteristics.

In most systems, degradation is caused by trapping of charge carriers in localized states in the organic semiconductor, gate dielectric, or at the interface between the two layers. The molecular-level nature of these defects and whether they are related to intrinsic structural defects or extrinsic chemical impurities or a combination thereof is still under investigation. The task of coming to a general understanding of reliability issues in OFETs[51] is complicated because there is a wide variety of organic

semiconductors with different chemical structures and varying levels of chemical purity.[9]

These factors, that lead to device degradation, modify the energetic landscape of the material and/or interface affecting the charge transport mechanism.[53] The corresponding effects are observed in the noise spectrum of conductivity fluctuations. The spectral features, in a PSD plot, are known to change with the density of trap states, applied field, free carrier concentration, thin film properties, etc. in organic electronics devices.[54,55] The magnitude of the noise spectrum, slope of frequency, and the dependence of noise spectrum on current or voltage are the indicators that help identify various mechanisms[26,36] that influence the charge transport properties and the observed noise in the device.

1.10 Outlook and Thesis Outline

In PFETs, various competing processes influence the charge transport mechanism and subsequently the current noise. Static or DC characteristics are helpful in determining the device performance parameters like mobility, on-off ratio, subthreshold swing (SS), leakage current and threshold voltage.[21] However, the time evolution of these properties is difficult to predict from these measurements. Low frequency noise analysis has been widely used as an analytical tool for improving device performance and to address reliability issues in Si-MOSFETs.[35,36] Noise measurements on OFETs have been reported using inorganic dielectric and organic semiconductor.[41,55–67] Studies in these systems provide limited insight into the transport properties of organic materials. A noise study reported by Kang et.al[68] used organic dielectric (PVP)[(i)] and semiconductor (pBTTT)[(j)] to study channel noise properties where the OTFT was fabricated on top of silicon dioxide. Another study by Jia et.al[69] deals with noise in parylene-C (organic dielectric) - pentacene (organic semiconductor) based OFETs, but Parylene-C requires a custom chemical vapor deposition chamber for obtaining thin films and is not solution processable. In this direction, the present study deals with current noise properties in polymer field effect transistors made from solution processable components and suitable for roll-to-roll

[(i)] poly-4-vinylphenol
[(j)] poly(2,5- bis(3-alkythiophen-2-yl)thieno[3,2-b]thiophene)

applications.

For a reliable noise measurement, it is important that external interference from surrounding be minimized. This demands a noise measurement environment which ensures effective shielding from external disturbances. The device fabrication procedure and the noise measurement technique are described in chapter-2 along with the details on data acquisition and digital signal processing techniques.

The third chapter is dedicated to the measurement and analysis of current noise in PFETs (both n-type and p-type). Noise in PFETs have been studied at different bias conditions and in different working regimes of transistor operation. This chapter is further divided into sections which deal with noise properties of different types of transistors at various biasing conditions. The first section deals with the current noise measured for n-type BCB-N2200[k]transistors while the second section deals with p-type BCB-P3HT transistors.

The third section forms the most important part of this thesis. The current noise properties of p-type PVDF-P3HT transistors are studied in detail, at different operating conditions. Current fluctuations have been studied both as a function of V_{gs} and V_{ds}. The subsequent section in this chapter deal with noise in transistors that have high gate leakage. The power spectrum corresponding to gate current noise and the channel noise compete in the total noise spectrum. At significantly high (gate) leakage, the corresponding noise spectrum shows features that can be correlated with magnitude of gate current in these devices.

The effect of light on the channel noise is studied in the last section. Upon illumination, the current noise, in the depletion mode of transistor operation, shows spectral features that are characteristic of noise originating from the bulk of the semiconductor. Photo-excitation of charge carriers influences the current magnitude in dark condition and the corresponding noise spectrum.

[k]the dielectric and semiconductor materials have been detailed in next chapter.

Chapter 2

Materials and Methods

The device fabrication procedure is critical in the field of organic electronics as fabrication of a working polymer field effect transistor (PFET) requires effort and practice. In order to investigate the noise properties of PFETs, it is crucial to work with a low-noise measurement set-up. External disturbances or unwanted noise may interfere with device output and contaminate signal "noise" data. Identifying possible noise sources are as important as reducing (or removing) them. Processing and fabrication details constitute the first half of this chapter and details regarding noise set-up and measurement, essential for a reliable noise analysis, are discussed in the second half.

2.1 Materials

The polymer field effect transistor (PFET) structure consists of disordered dielectric layer, semiconductor layer and electrodes. A brief description of these material components is described in following sections.

2.1.1 Dielectric Materials

(a) Benzocyclobutene (BCB)

Divinyltetramethyldisilooxane-bis (benzocyclobutene) (DVS-bis-BCB) is an organic dielectric, having a dielectric constant of 2.65, derived from BCB. It has been used as the gate insulator in the PFET structure. It is diluted in a 1:1 ratio with filtered

mesitylene (spectroscopic grade). Thin films are obtained on cleaned glass substrates by spin coating the diluted solution at 800 rpm for 1 minute, including 10 seconds ramp-up time from 0 to 800 rpm. The curing temperature for BCB is 250^0C beyond which the molecules get cross-linked forming a dense polymer network.[70] The spin coating procedure is followed by thermal annealing (hard bake) at 290^0C inside Glove-box[(a)]for 1 hour. BCB gives highly transparent thin films and has very less leakage (few to tens of pA) due to high volume resistivity ($\sim 10^{18}\ \Omega - cm$). The breakdown voltage is approximately 5 MV/cm or 0.5 V/nm which is suitable for OFETs since they have high operating voltages. The typical thickness obtained after annealing is around 200 nm.

(b) Poly-vinylidene fluoride (PVDF)

Polyvinylidene fluoride (PVDF) is a non-reactive and thermoplastic fluoropolymer produced by the polymerization of vinylidene difluoride. The dielectric constant is $\sim$ 7.4 with a dielectric strength of 0.18 MV/cm. The volume resistivity is $\sim 10^{14}\Omega.cm$, which is less compared to BCB thus the gate current leakage is more pronounced in PVDF based PFETs. Thin films are obtained by spin coating at 800 rpm for 1 minute from a solution of PVDF in Dimethylformamide (DMF) having a concentration of 80 mg/ml. It is followed by thermal annealing at 140^0C in an inert atmosphere. Typical thickness obtained is in the range of 300 - 400 nm.

2.1.2 Organic Semiconductors

(a) Poly-3-hexyl thiophene (P3HT)

Poly-3-hexyl thiophene (P3HT), the model semiconductor, is used for noise studies in PFET structure. It belongs to a group of alkyl substituted poly-thiophenes (P3AT) and has been extensively studied. The HOMO and LUMO levels lie close to -5 eV and -3 eV, respectively.[71] High molecular weight regio-regular(rr) P3HT ($\sim 88k$) is used for making PFETs; higher molecular weight of polymers are characteristic of long polymer backbone.[15] Thin films are obtained by spin coating P3HT solution (10 mg/ml in anhydrous chlorobenzene) at 800 rpm for 1 min. on top of

[(a)] Glove-box provides an inert (N_2) atmosphere having O_2 and H_2O concentration less than 10 ppm and 5 ppm, respectively.

a dielectric layer, followed by thermal annealing for 1 hour at 110^0C in an inert atmosphere. For BCB based devices, a thin layer of Hexamethyldisilazane (HMDS) is also spin-coated on top of (annealed) BCB layer to passivate the dielectric surface and reduce electron trap states at the dielectric-semiconductor interface.

***(b)* N2200**

NDI-based polymer poly[N,N'-bis(2-octyldodecyl)-naphthalene-1,4,5,8-bis(dicarboximide)-2,6-diyl]-alt-5,5'-(2,2'-bithiophene) or N2200 is used as a n-type semiconductor in PFETs. Thin film are obtained by spin coating at 1000 rpm for 1 min. (5 mg/ml solution in anhydrous chlorobenzene) and annealed at 140^0C for 2 hours.

2.2 Device Fabrication

Transistors are made in bottom-gate top-contact (BGTC) architecture (fig.1.1b) on a cleaned glass substrate. The steps involved in the fabrication of a PFET are explained below:

- ***Substrate Cleaning:*** Glass substrates have been cleaned by multiple rounds of ultrasonication followed by standard RCA procedure. After every round of cleaning, the substrates are blow dried with nitrogen. A 1:1 mixture of isopropyl alcohol (IPA) and acetone is used for ultrasonication which is followed by rinsing substrates in running deionised (DI) water. RCA cleaning involves heating glass substrates in a 1:1:5 mixture of ammonium hydroxide, hydrogen peroxide and DI water, respectively, at $\sim 90^0C$ till the effervescence disappears (typically 15 - 20 minutes). Finally, the cleaned substrates are sonicated in DI water and baked in an oven at $\sim 50^0C$, for half an hour, to remove any trace quantities of water.

- ***Gate Electrode:*** Aluminium (Al.) is used as the gate electrode for P3HT based transistors and is coated on top of cleaned glass substrates by thermal evaporation. Al. is coated at a rate of $1A^0/s$ when the pressure inside the thermal evaporation chamber is $2 \times 10^{-6} mbar$ or less. The gate area is patterned using a shadow mask, using Teflon (polytetrafluoroethylene).

- ***Thin Films coating:*** Gate electrode coated substrates are transferred to Glove box for thin film coatings of dielectric and semiconductor. The solution processable dielectric and semiconductor are deposited by spin-coating at optimised speeds (mentioned in section 2.1). Each spin coated layer is followed by a thermal annealing process and subsequently cooled down to room temperature.

- ***Source-Drain Electrodes:*** Top contact source-drain electrodes are coated similar to gate electrode. Gold (Au) is used for p-type semiconductor (P3HT) while Al. for n-type semiconductor (N2200).

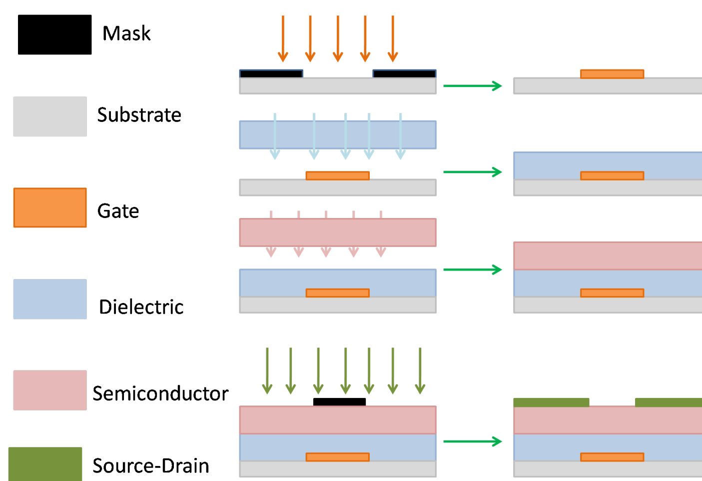

Figure 2.1: Schematic diagram showing steps of device fabrication

2.3 DC Characterisation

The transistor I-V characteristics and capacitance measurements (capacitance-voltage and capacitance-frequency) are done using Keithley 4200-SCS parameter analyzer. Automated library functions are used for all the measurements. The value obtained from these measurements is used in noise analysis. It is generally observed that the current characteristics change with sweep rate and the applied bias time. In noise measurement, bias is applied to transistors typically for few (5-10) seconds and the current values may differ with I-V curves obtained from the parameter analyzer. It is observed that sample time of 2 seconds and hold time of 1-second show similar

current levels. Further, I-V measurements are taken before and after the noise measurement to check for drift in transistor performance. Devices which show very less drift and hysteresis are chosen for noise studies.

2.4 Noise Setup

External noise or disturbances interfere with the system under investigation and obscure the low-level signals from the device. The electrical noise can be induced, in wires, cables and connections, due to electromagnetic interference or due to vibration effects. Controlling these unwanted signals and keeping it within acceptable limits is vital to any data acquisition system. For designing a low-noise measurement setup, it is important to identify the main sources of noise and then design strategies to reduce them, as far as possible.

2.4.1 Sources of Noise

Most laboratories and industrial environments contain abundant electrical noise sources which include AC power lines, heavy machinery (like motors, vacuum pumps), radio and TV stations, and a variety of electronic equipment. Radio stations generate high-frequency noise while computers and other electronic equipment generate noise in all frequency ranges. Noise sources having a specific frequency appear as sharp peak in the power spectrum and can be identified, for example, peaks at 50/60 Hz and its harmonics are due to the power line, and a peak at 2.4 GHz corresponds to wi-fi and Bluetooth operation. For sources which generate noise in a wide range of frequency, it is better to isolate and decouple them from the instrumentation setup.

Noise can couple into electric circuits by various means and a careful understanding of coupling methods can help eliminate them. Most commonly the noise couples into a circuit on a conductor. A wire running through a noisy environment may pick up spurious signals and then conduct it to another circuit. Most common example of this *conductively coupled noise* is noise conducted into a circuit through power supply leads.

Radiated electric and magnetic fields are other means of noise coupling.

All circuit elements including conductors radiate electromagnetic waves whenever a charge is moved. In addition to this unintentional radiation, there is the problem of intentional sources such as the radio broadcast station, radar transmitters and wireless communication waves in the form wi-fi and Bluetooth signals.

The grounding conflict: Preventing electrical shocks and electrical fires is the highest priority for ground circuits, but these redundancies (of ground connections) built into many electrical grounding systems create a conflict with data acquisition systems called as ground loops. A ground loop can be understood as multiple paths for ground currents. Several internal, common busses in a data control instrument are arranged to regulate current flows and terminate all paths at one common point. Usually, this one common point connects through a low impedance to the safety ground connection, on the instruments AC power cord. This connection prevents the internal system from floating at an AC potential between earth ground and the input AC supply potential. Measuring instruments that contain an earth ground, as described above, usually generate a ground loop. A ground loop can become a serious problem even when the ground voltage on the measured point equals the ground voltage entering the instrument through the line cord. A voltage that develops between the two grounds can be either an AC or a DC voltage of any value and frequency, and as the voltage and frequency increase, the ground loop becomes more troublesome and dominates the input waveforms in noise measurements.

Triboelectric Effect: A charge can be produced on the dielectric material within a cable if the dielectric doesn't maintain contact with the cable conductors. This is called the triboelectric effect. It is usually caused by mechanical bending of the cable or if the cable is simply hanging without any rigid support. The charge acts as a noise voltage within the cable and adds up with the DUT signal.

Conductor Motion: If a wire is moved through a magnetic field, a voltage is induced between the ends of the wire. Due to power wiring and other circuits with high current, in laboratories and industries, stray magnetic fields exist in most environments. If a wire with a low-level signal is then allowed to move through this field, a noise voltage is induced in the wire. The problem can be especially troublesome in a vibrational environment.

2.4.2 Noise Reduction

After careful inspection of possible noise sources, a set-up has been designed taking proper precautions which are suited for noise measurements. The first and foremost thing for minimizing environmental (electromagnetic) interference is to have a ***shielded metal enclosure***, also known as ***faraday cage***. The faraday cage in this setup has been made from 2mm thick aluminium sheet having a cubic shape of side length 20 inches. Shielding is very important when the circuit connections have unshielded metal wires and connections. The faraday cage houses the device under test (DUT) as well as the DC biasing circuit.

The solution for *conductively coupled noise* is to prevent it from entering the signal path before it interferes with the susceptible circuit. If other instruments are connected to the power supply which generates noise, it becomes necessary to decouple noise from the wires before they enter the circuit. Here the biasing circuit for OFET is made from a combination of sealed lead acid batteries for all ranges of measurement. Using an isolated DC voltage source gives an advantage over AC power supply as it completely eliminates power line interference and associated noise on power leads.

The ground loop problem is avoided by having a single grounding contact at the dynamic signal analyzer (DSA). Connections from DUT and preamplifier are grounded with DSA channel input (using BNC coaxial cables), while the faraday cage is separately grounded to the instrument's ground connection port by a thick copper wire. The outer shield of BNC cables (from the DUT) are not shorted with the metal shield to avoid ground loops. Further, the instrument ground is physically isolated from the rest of the instruments by having a separate ground line to the earth.

The DUT is placed in a diecast aluminium box (G106) for better shielding which also provides a very low resistance to common ground connections at the DUT and DC bias. BNC female connectors are fitted into the metal box and copper wires soldered to the connector's centre pin for taking contacts with the DUT. These copper wires take the connection from the electrodes of DUT and are made firm by the use of conducting silver paste. No pressure is applied in these contacts. The silver paste, used here, is a dispersion of micron-sized (0.5 microns or less) fine silver

particles in amyl acetate. After making the connections, the box is covered with a lid and tightened. This ensures reliable electrical and optical shielding of the sample.

To minimize vibration induced noise in the circuit, the entire setup is kept on a vibration proof table. The noise in cables due to triboelectric effect is minimized by avoiding cable movement and keeping them steady, and eliminating sharp bends while making connections. Short cable lengths (1 metre) are used for connections, to avoid extra noise sources.

2.5 Instrument Configuration

The instruments which are a part of the measurement setup comprises of a dynamic signal analyser and a low noise transimpedance amplifer. The settings and configuration that are essential for a reliable noise measurement are discussed in subsequent sections.

- ***Dynamic Signal Analyser (DSA)***
- ***Transimpedance amplifier (TIA)***

2.5.1 Transimpedance amplifier (TIA)

A current to voltage preamplifier is used to amplify the (current) signal from DUT. The TIA used in noise studies are DLPCA 200 (Femto) and SR 570 (Stanfard Research Systems). Typical settings of a current amplifier, for noise measurement, are explained below.

- **Input current:** The amplifier is connected in series with the device (DUT) and so the current flows through the front-end input of the TIA. There is a limitation to the current magnitude at a particular gain setting. For both TIAs, the maximum input current that can be passed through the TIA scales down with gain. The corresponding values are listed in the datasheet of the instruments.

- **Transimpedance gain:** is defined as the ratio of the output voltage to the input current. A high gain implies large amplification of the input signal.

The gain of an amplifier is inversely related to its bandwidth, in terms of gain-bandwidth (GBW) product which is constant over a certain range of frequency. This means that bandwidth reduces when gain is increased and vice versa. It is advisable to keep the gain at a value which is close to the inverse of the DUT resistance for optimum performance. Gain is referred to as sensitivity in SR 570, a sensitivity of $10^{-3}A/V$ is equivalent to a transimpedance gain of $10^{3}V/A$. The gain settings should be adjusted keeping in mind, the input DC current and the frequency range that is required.

- **Bandwidth:** The upper 3-db cut-off frequency (or the bandwidth) is limited by gain settings. Like the maximum input current, the bandwidth also reduces with gain. Typically it reduces from $1.0MHz$ (sensitivity of $10^{-3}A/V$) to $10Hz$ (sensitivity $10^{-9}A/V$) in SR 570, whereas for Femto it reduces from $500kHz$ to $1.1kHz$ at similar gain settings. The amplifier response is linear in a given bandwidth and rolls off at higher frequencies. This feature should be taken into account to avoid error in data analysis.

- **Coupling:** The choice of coupling is optional and is required only when the amplifier's DC bias is to be connected in series with DUT in the circuit. For most amplification purposes, the input coupling is kept at "Ground" setting. The voltage output can be AC or DC coupled, DC coupling is the normal mode of operation while in AC coupling a capacitor is placed in the circuit which removes the DC components (frequency close to zero).

- **Precautions:** Proper care and attention should be taken while using current amplifier in a noise measurement. Unmatched settings can lead to erroneous results and/or instrument failure. The value of the maximum DC current that can be present in the circuit should be taken into account while setting the gain. When the current exceeds the maximum allowable current, an "Overload" condition is reached which is seen as the glowing of a red LED indicator on the display panel. This condition should be avoided as much as possible. In occurrence of such an event, the connection from the DUT or the circuit should be terminated immediately to avoid severe instrument damage. The input coupling should be kept at "Ground" by default and the DC bias kept

at low values to avoid accidental flow of large currents through its input terminals, when low impedance DUTs are connected. Apart from these, other settings that are specific to the experiment like bandwidth, filter cut-off, input current noise, output coupling, etc. should be factored into data analysis.

2.5.2 Dynamic Signal Analyser (DSA)

The Agilent 35670A dynamic signal analyser (DSA) is a low noise 16-bit "fft" spectrum analyser that samples and stores voltage signal. Key-points regarding the operation of DSA, that is fundamental for making a reliable noise measurement, are explained below.

- **Input coupling:** The input to DSA should be properly configured before sampling. The choice of ground or float coupling is dictated by the physical grounding of the electronic circuit. The noise measurements, in this thesis, have DSA as the single grounding point in the circuit and so the input is ground coupled with the input channel. Apart from that, AC coupling is used to sample the fluctuations or noise in the voltage output from amplifier.

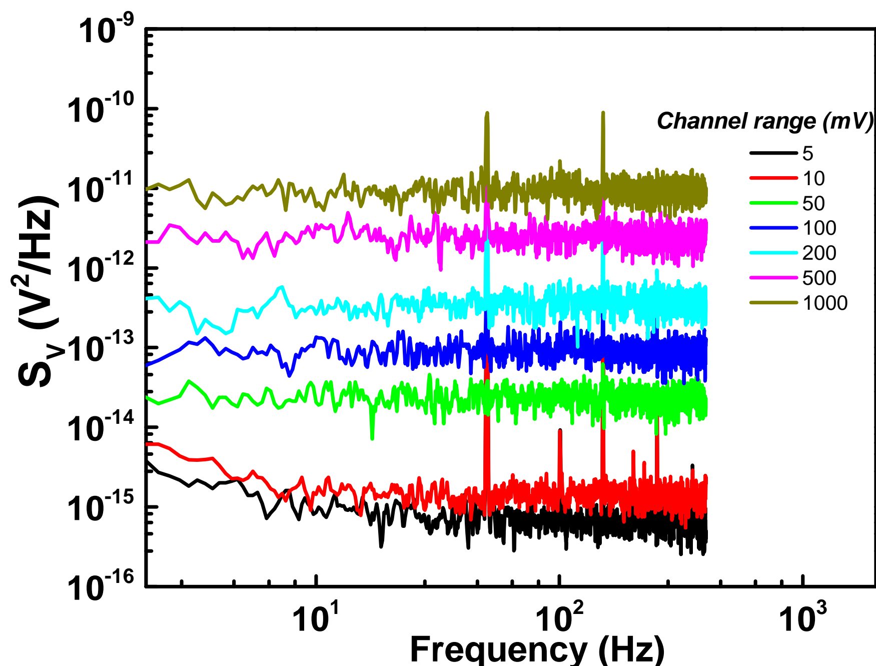

Figure 2.2: Power spectrum of channel noise at different levels of input range.

The channel input range (peak-to-peak voltage V_{pp}) for voltage signals is user defined and should be adjusted by taking into account the largest peak-to-peak values of the input voltage (V_{in}) signals (which are output from TIA). The ability of DSA to resolve the smallest voltage signal is determined the number of bits (16) of ADC at the front-end and the selected input range. For the minimum possible V_{pp} range of 4 mV at DSA, the lowest value of V_{in} that can be faithfully detected is given by the relation,

$$V_{in} = \frac{V_{pp}(4 \times 10^{-3})}{2^{16}} \approx 6 \times 10^{-8} V$$

Thus, the voltage (energy) spectral density would be $\sim 10^{-15}\ V^2$. The power spectrum density is expected to be in similar range, however, it is frequency dependent and decreases at higher frequencies. The channel input digitization noise is a practical bottleneck for measuring low noise signals and so the signals are amplified before digital sampling to surpass the noise floor of the instrument. It can also be seen from the above equation that the channel input noise scales up with channel range (fig.2.2). The channel range should be such that smaller values don't lead to overload conditions and higher values don't overwhelm DUT noise.

- **Frequency Span:** The bandwidth (BW) of the DSA is DC to 102.4 kHz. This means that the higher frequency f_h limit is 102.4 kHz while the lower frequency (f_l) depends on the total sampling time duration (T) and is limited by the low frequency noise of the instrument. The upper frequency can be adjusted in powers of 2 descending from 102.4 kHz while the lower frequency is adjusted by the number of resolution lines. The sampling frequency f_s is adjusted by DSA automatically corresponding to user defined f_h, while maintaining the Nyquist criterion. The mathematical relations for signal processing by DSA are given below.

$$f_l = 1/T \qquad \text{frequency span}, f_{span} = f_h - f_l \qquad f_s = 2.56 \times f_h$$

Usually f_h is dictated by BW at TIA but higher frequencies can also be chosen to have higher sampling frequencies, for better resolution, in frequency

response.

- **Resolution lines:** The ability to resolve two signals at closely spaced frequencies depends on the frequency resolution of the spectrum. The number of resolution lines, in DSA, is responsible for the frequency resolution (f_{res}) in the power spectrum plot. It can take values of 400, 800 and 1600 (used for noise measurements). In one time capture frame, the lower frequency at DSA is defined by resolution lines.

  $$f_l = \frac{f_h(1.6kHz)}{lines(1600)} = f_l(1Hz)$$

  where, minimum frequency resolution, $f_{res} = f_l$. Smaller the magnitude of f_{res} , higher is the resolution.

  The time span (Δt) of capturing one data frame is defined by f_l, as $\Delta t = 1/f_l$. Usually y ($\sim$ 50) frames are captured for averaging the plots and in that case, $T = y\Delta t$.

- **Data Processing:** The instrument can be used in two modes after it is configured for data analysis. In the first mode, the time series capture of data (voltage v/s time) is stored in the buffer memory and subsequently transferred into a desktop for further analysis. The maximum number of data points, that can be saved in one capture, is determined by the buffer memory of DSA[(b)]. In the second mode, the power spectrum is computed and averaged directly by the instrument, as per the user-defined settings and subsequently stored into a computer. For the time series data, all of the digital signal processing, for time and frequency domain analysis, is done in Matlab (R2008b). The code used for this purpose is given in Appendix-A.

- **Precautions:** Like the TIA, the instrument channel should be protected from voltage signals that are greater than the channel input range. At low levels of signal input, the range can be in *auto-range* mode to avoid such problems, but it is often required to have a constant thermal noise floor of the background setup. In that case, the channel range should be adjusted corresponding to

[(b)] with the available memory, typically 10 mega-points can be saved

the maximum current or voltage produced in the circuit. The input cables should be immediately disconnected in the event of an unexpected spike in voltage levels. The instruments should be monitored during a measurement for indications of "overload" condition.

2.6 Noise measurement

The DUT (PFET) for noise measurement is a three terminal device. The gate and drain terminals are used for biasing the transistor whereas source is used for collecting current.

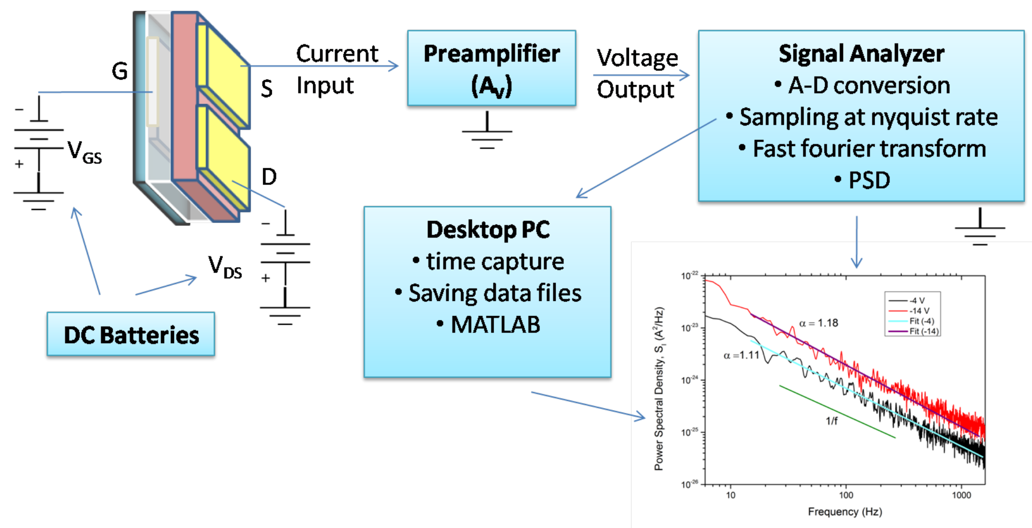

Figure 2.3: Schematic of the circuit for transistor noise measurement.

Sealed lead acid batteries are used for biasing the DUT and are placed inside the faraday cage. The voltage output from TIA can be stored in a digital format in an oscilloscope or DSA. The accuracy and background noise level is related to the number of bits used for analog-to-digital conversion of input signals. The DSA is preferred over the 8-bit oscilloscope (LeCroy WaveRunner 6100A) for low frequency noise measurements. The circuit connection and the signal path is shown in fig.2.3. Data collected from DSA is processed on a desktop PC using Matlab.

Chapter 3

Noise Studies

It has been known that transistor performance is correlated to the magnitude of low frequency noise[46,56,57,63,69,72–74] present in the output current. The channel current fluctuations in (p-type and n-type) OFETs are studied in this chapter, to understand the transport properties and to address stability issues. The current noise has been measured for linear and saturation regimes of transistor operation, at different bias conditions. The gate referred input current noise is studied for different (p-type) devices that show varying levels of leakage gate current. The noise properties of channel current are also measured for steady state light illumination, in the depletion mode of transistor operation.

3.1 Experiments and measurements

To study noise in high resistance ($> 1M\Omega$) devices, the current is amplified using a low input impedance (50-100 Ω) current-to-voltage amplifier. For low resistance ($<$10 $k\Omega$)devices, the voltage drop across a load resistor is amplified using a voltage-voltage amplifier. In an alternate approach, the device is used as the arms of balanced wheatstone bridge network and fluctuations through the balanced arm amplified using lock-in amplifier, commonly referred to as the ***a.c.*** or ***lock-in*** technique.[75,76] In case of OFETs, the channel resistance range from few to tens of $M\Omega$s, and so current amplification is preferred for noise measurements. The noise studies for n-type and p-type OFETs are presented in this section.

n-type transistors

3.1.1 BCB-N2200 transistors

OFETs were fabricated using BCB as gate dielectric and N2200 as semiconductor[(a)]. These OFETs function as n-type transistor when sufficient positive bias is applied to gate and drain terminals. Aluminium is used as SD electrodes[77] to match the work function of electrode with that of HOMO level of semiconductor.

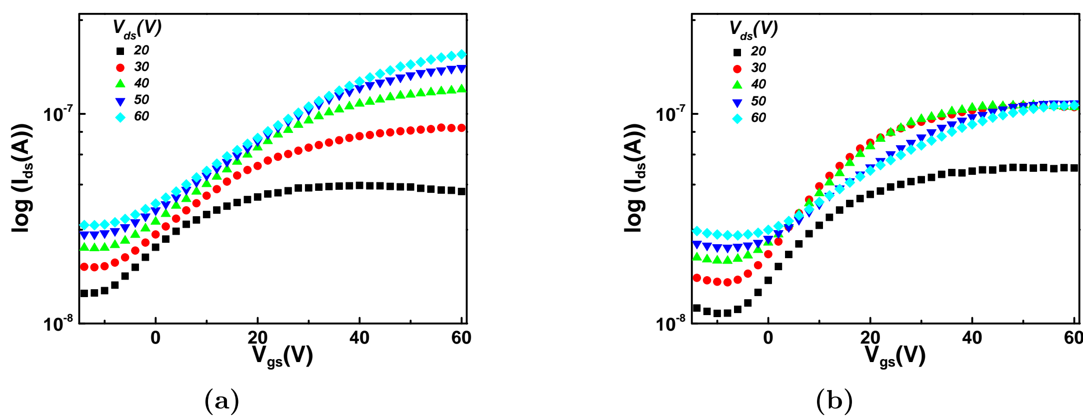

Figure 3.1: Source-drain current plotted as a function of gate bias (transfer curve) at different drain bias (V_{ds}), for n-type BCB-N2200 (BN) transistor before (fig-(a))and after (fig-(b)) the noise measurement.

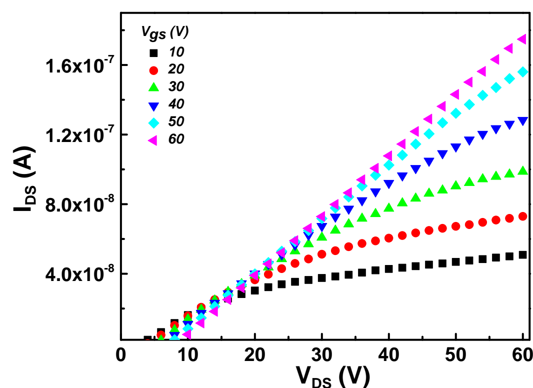

Figure 3.2: Source-drain current plotted as a function of drain bias (output curve) at different gate bias (V_{gs}), for n-type BCB-N2200 transistor in fig-3.1. Channel length, L = 60 microns and width W= 0.91 mm.

[(a)]in short form, these devices will be referred as BN transistors.

From fig-3.1 and 3.2, it is observed that DC characteristics of BN transistors lack distinct linear and saturation regimes. Similar behaviour was observed for other transistors (8 devices) as well. However, the SD current shows a gate dependence and noise measurements were carried out for these devices.

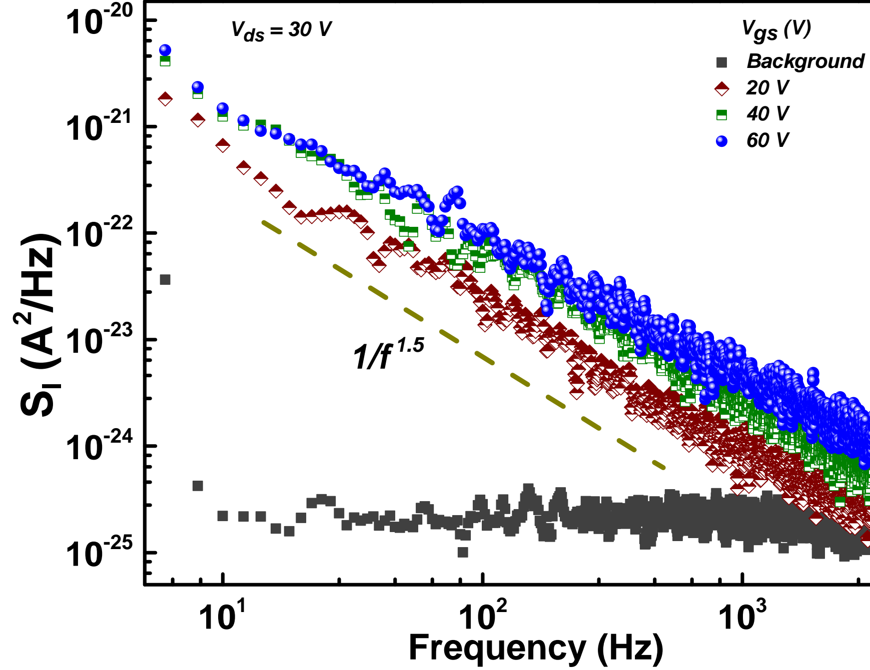

Figure 3.3: Current noise spectrum of a BCB-N2200 transistor plotted as a function of frequency, at different gate bias. A reference 1/f-type plot with slope 1.5 is shown in dashed line.

To study noise in BN transistors, channel current was measured at $V_{ds} = 30V$ while V_{gs} was varied from 20 V to 60 V (in steps of 10 V). The experiment details corresponding to this set of measurements are detailed below:

- Transimpedance gain at preamplifier : 10^6 V/A
- Measured frequency range: 2 Hz to 3.2 kHz
- Time duration for capture of one data-frame: 0.5 second
- Number of data-frames in one dataset: 50
- Devices were encapsulated and measured in dark conditions, at room temperature (298 K)

- Gate and drain terminals were kept at ground potential after every measurement.
- Hold time of 60 - 80 seconds between successive measurements.

The noise spectrum is analysed using modified Hooge's empirical relation (1.18) given by,

$$S_I(f) = \gamma_H I^\beta / N f^\alpha$$

For BN transistors, the current power spectrum density (PSD) shows a $1/f^\alpha$ type behaviour (fig.3.3) at different V_{gs}. The frequency exponent, α lies close to 1.4 (1.4 $\pm$ 0.2). The DC characteristics of these transistors have been observed to change drastically and show significant drift, before and after the noise measurement (fig-3.1). The analysis of noise spectrum becomes complex, in situations, where the mean current (I) has a transient behaviour during the measurement.[27] Further noise studies were not carried out for BN devices due to the lack of stable and working transistors.

p-type transistors

3.1.2 BCB-P3HT transistors

The OFETs studied in this section were fabricated using BCB dielectric and P3HT semiconductor[(b)]. The transistors function as p-type OFET when sufficient negative bias is applied to gate and drain terminals. Gold is used as SD electrodes to match the electrode work-function with that of LUMO level of the semiconductor.[78]

[(b)] in short form, these devices will be referred as BP transistors.

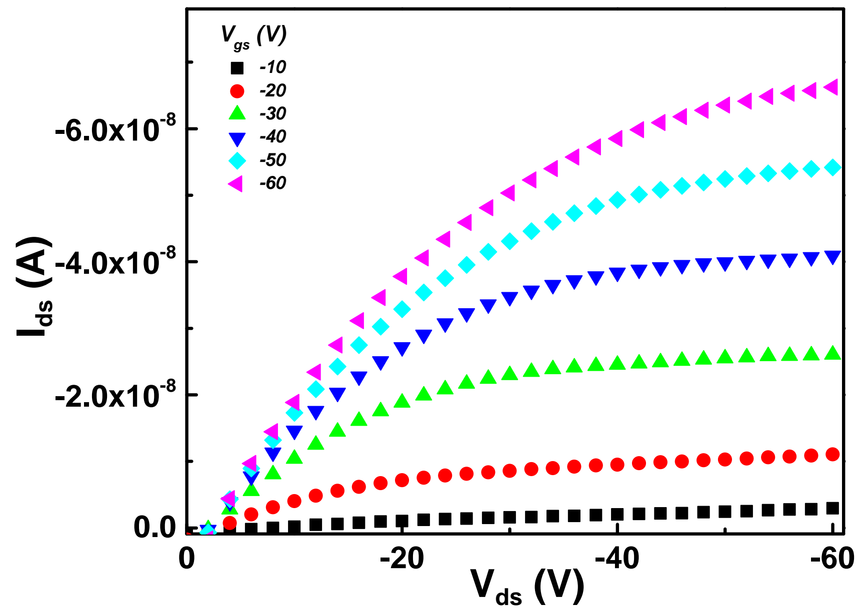

Figure 3.4: Source-drain current plotted as a function of drain bias (output curve) at different gate bias (V_{gs}), for a p-type BCB-P3HT transistor.

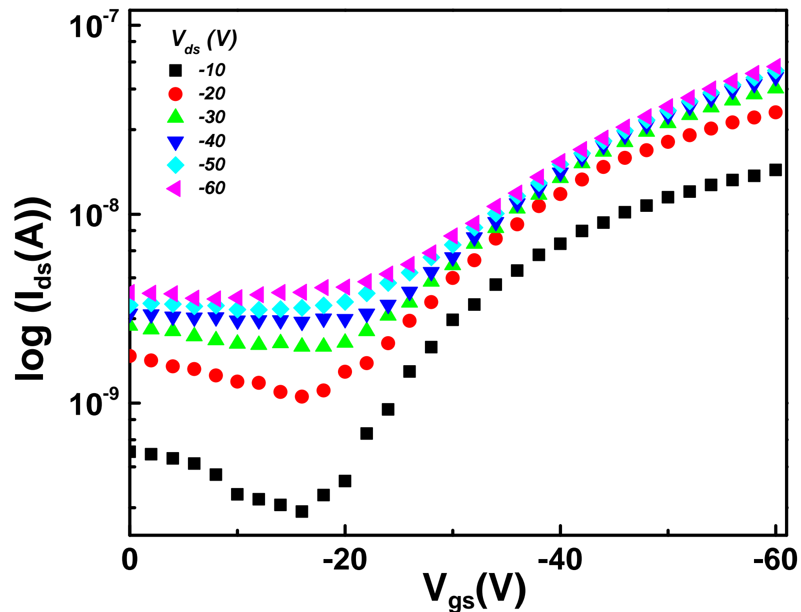

Figure 3.5: Source-drain current plotted as a function of gate bias (transfer curve) at different drain bias (V_{ds}), for the p-type BCB-P3HT transistor in fig-3.4. Channel length, L = 50 microns and width W= 0.9 mm.

The DC characteristics of BP transistors showed a gradual shift with operating time, but the shape of plot remained the same, showing clear linear and saturation regimes (fig-3.4). Devices having minimum drift in DC characteristics were chosen for noise studies. The current noise is investigated for such transistors, in the linear regime, at different V_{ds}.

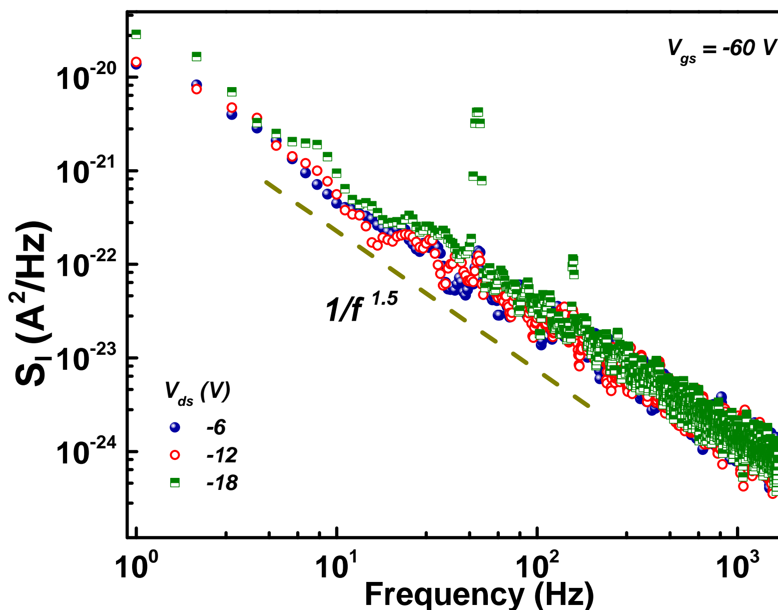

Figure 3.6: Current noise spectrum of a BCB-P3HT transistor plotted as a function of frequency, at different drain bias. The gate bias is kept constant at $V_{gs} = -60V$. A reference $1/f^{\alpha}$ type plot with $\alpha = 1.5$ is shown in dashed line.

The experiment details for this noise study are mentioned below:

- V_{gs}= -60 V
- V_{ds} varied from -6 V to -20 V in steps of -2 V (8 data sets)
- Transimpedance gain at preamplifier : 10^6 V/A
- Measured frequency range: 1 Hz to 1.6 kHz
- Time duration for capture of one data-frame: 1 second
- Number of data-frames in one dataset: 40
- Devices were encapsulated and measured in dark conditions, at room temperature (298 K).

- Gate and drain terminals were kept at ground potential after every measurement.

- Hold time of 60 - 80 seconds between successive measurements.

The noise characteristics of BP transistor have been shown in fig-3.6. The power spectrum density in linear regime exhibits a $1/f^{\alpha}$ type behaviour with frequency exponent, $\alpha \sim 1.4$ (1.4 ± 0.1). The peaks at 50 Hz and 100 Hz (PSD plot for $V_{ds} = -18V$) are due to noise from power line supply.

The noise magnitude, here, is independent of the mean current value (or V_{ds}). According to Hooge relation (eqn.1.16), the noise power spectrum has a current bias dependence[39] characterized by exponent β (= 2),however, in the present case β is almost zero. Such behaviour in power spectrum are difficult to explain quantitatively, and may result due to some parasitic noise source in the channel or the bulk of semiconductor, which dominates the total noise spectrum. Measurement on other BP transistors (5 devices) showed similar behaviour.

3.1.3 PVDF-P3HT transistors

The p-type transistors based on PVDF (dielectric) and P3HT (semiconductor)[(c)] have been studied in this section. Representative set of typical output and transfer curves of a PP transistor, chosen for noise studies, are shown in fig.3.8 and 3.7, respectively. These transistors showed stable DC characteristics for measurements over a long period of time ($\sim$ 3 weeks), and were studied in detail.

The output curve (fig-3.7) show distinct linear and saturation regime. Transfer curve for V_{ds} = -60 V is plotted, (fig-3.9) to obtain threshold voltage and for the calculation of saturation mobility. The linear fit to $\sqrt{I_{ds}}$ v/s V_{gs} plot when extrapolated to $I_{ds} = 0$ gives the threshold voltage ($V_{th} = -15V$). The saturation mobility, μ_{sat} is obtained by calculating the slope from the linear fit. For PP transistors, μ_{sat} typically lies in the range $10^{-4} - 10^{-3}$ $cm^2V^{-1}s^{-1}$. A number of devices (> 100) were measured to check for the stability of DC characteristics, and those showing minimum hysteresis and drift (15 devices) were further studied to investigate noise properties.

[(c)] here after, referred to as PP transistors in this chapter

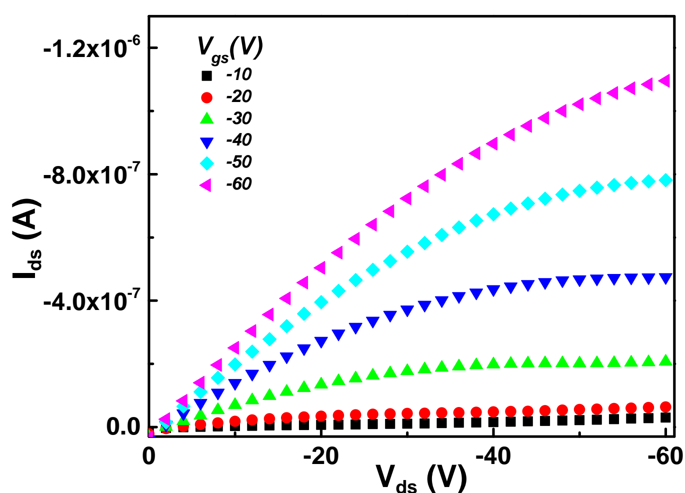

Figure 3.7: Source-drain current plotted as a function of drain bias (output curve) at different gate bias, for a p-type PVDF-P3HT (PP) transistor. The channel length $L = 30$ microns and channel width $W = 0.84$ mm.

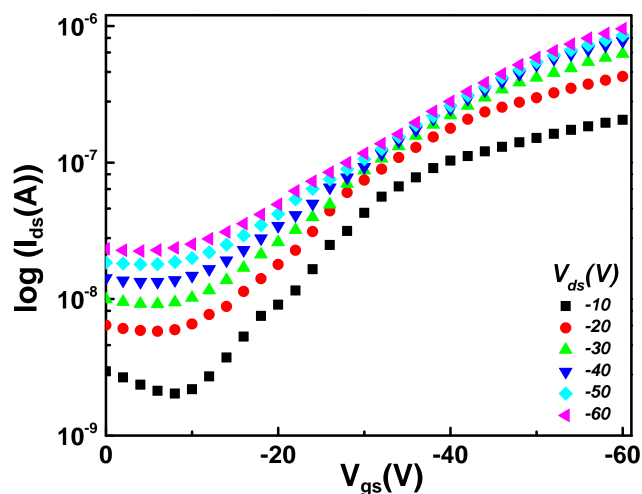

Figure 3.8: Source-drain current plotted as a function of gate bias (transfer curve) at different drain bias, for the p-type PVDF-P3HT (PP) transistor in fig-3.7.

The experimental conditions for noise measurements on PP transistors are mentioned below:

- Transimpedance gain at preamplifier : 10^6 V/A
- Measured frequency range: 1 Hz to 1.6 kHz
- Time duration for capture of one data-frame: 1 second
- Number of data-frames in one dataset: 40

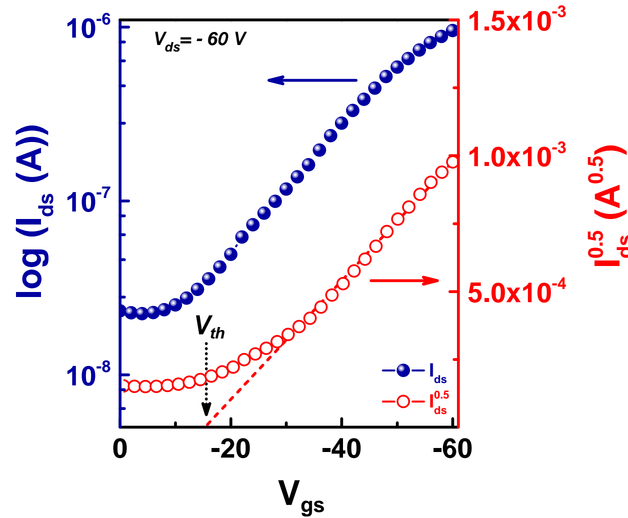

Figure 3.9: Square root (Y-axis right) and log scale (Y-axis left) plot of drain current v/s gate voltage (at $V_{ds} - 60V$) for a p-type PVDF-P3HT transistor (fig-3.7). The linear fit to the plot corresponding to $I_{ds}^{0.5}$ is shown in dashed lines which gives threshold voltage, V_{th} -15 V.

- Devices were encapsulated and measured in dark conditions, at room temperature (298 K).
- Gate and drain terminals were kept at ground potential after every measurement.
- Hold time of 60 - 80 seconds between successive measurements.

The current noise of these OFETs are studied at different bias conditions and are detailed in subsequent sections.

(a) Drain voltage dependence of noise

In this section, current noise spectra is measured in linear regime by varying V_{ds} from -4 V to -24 V (steps of -2 V) and keeping V_{gs} constant at -60 V. The DC characteristics of the transistor are shown in fig-3.7 and fig-3.8.

The PSD for this study shows a typical $1/f^{\alpha}$ type behaviour (fig.3.10) in the measured frequency range. The spectral features are analysed by using the Hooge empirical equation (eqn-1.18). Here, the frequency exponent α is close to 1 (1 ± 0.1). It is observed that noise magnitude increases with the drain bias (or I_{ds}).

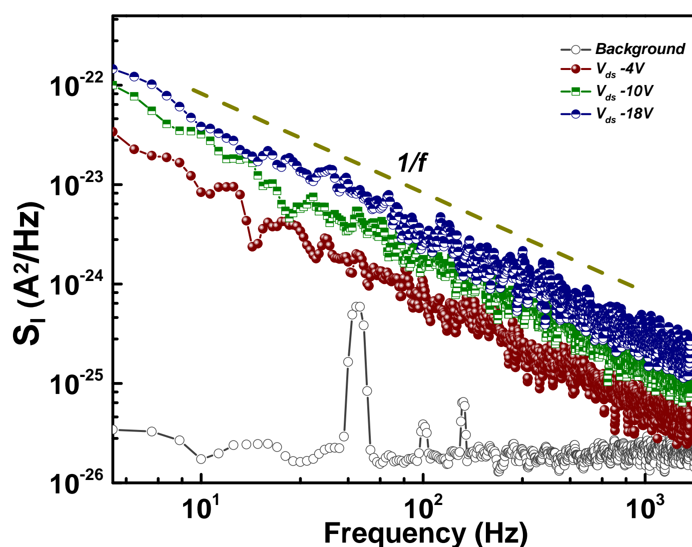

Figure 3.10: Current noise spectrum ($S_I(f)$) plotted as a function of frequency, in linear regime at different drain voltage and constant V_{gs} (-60V) for a p-type PVDF-P3HT transistor (fig-3.7). The dashed line shows a reference 1/f plot.

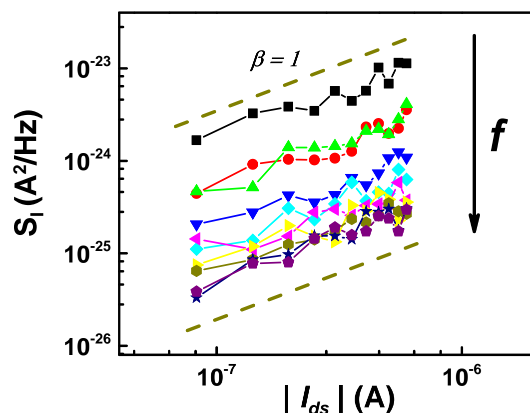

Figure 3.11: Current noise spectrum ($S_I(f)$) plotted as a function of current magnitude for a p-type PVDF-P3HT transistor (fig-3.10). The transistor is operated in linear regime, gate voltage is at -60 V and drain voltage varied from -4 V to -24 V. The dashed lines show reference slope corresponding to current exponent β=1, in the Hooge relation.

The current dependence of noise spectrum (β) is obtained from log-log plot of PSD ($S_I(f)$) as a function of drain current (I_{ds}), and is shown in fig-3.11. It is observed that β lies close to unity (0.9 ± 0.1).

(b) Gate voltage dependence of noise

In linear regime

In this study, V_{ds} is kept below V_{gs}^{eff} and SD current (I_{ds}) is measured at different values of V_{gs} for calculating noise. The DC characteristics of the PP transistor[(d)], used in this study, are similar to that in fig-3.7 with a threshold voltage V_{th} = -15V.

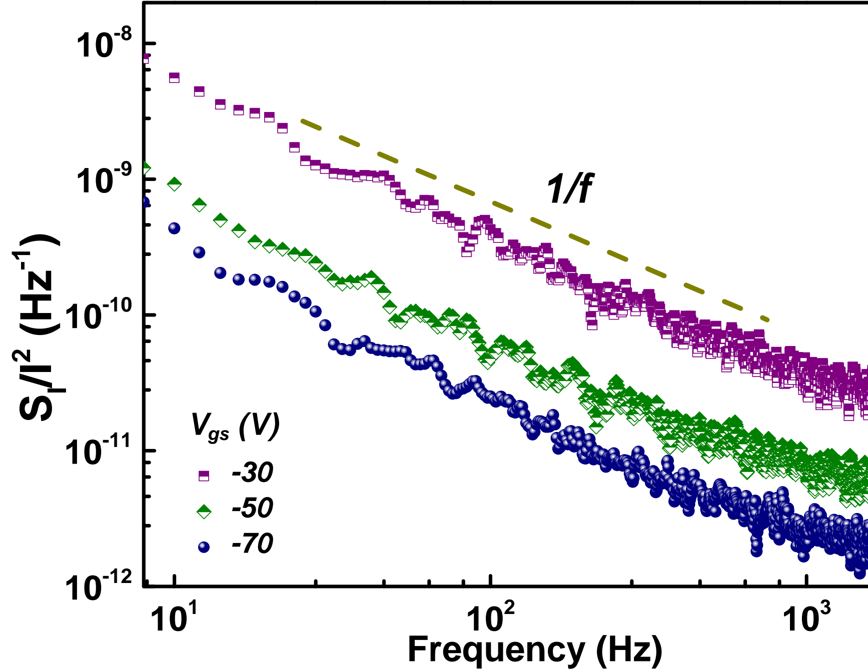

Figure 3.12: Normalised power spectral density ($S(f)$) plotted as a function of frequency for a p-type PVDF-P3HT transistor. The transistor is operated in linear regime at different gate voltage and constant V_{ds} (-10V) The dashed line shows a reference 1/f plot.

The current noise spectra, in linear regime (fig.3.12), is measured at different V_{gs} ranging from -30V to -70V (steps of -10 V), at constant V_{ds} (-10V). The PSD exhibits a $1/f^{\alpha}$ type behaviour where the frequency exponent, α is close to 1 (1 ± 0.1).

The gate voltage dependence of current spectrum (eqn.1.14 and 1.25) is obtained by calculating exponent p in the following relation

$$S(f) = \frac{S_I(f)}{I^2} \propto \frac{1}{(V_{gs}^{eff})^p} \tag{3.1}$$

[(d)] L=60 microns and W= 1.13 mm

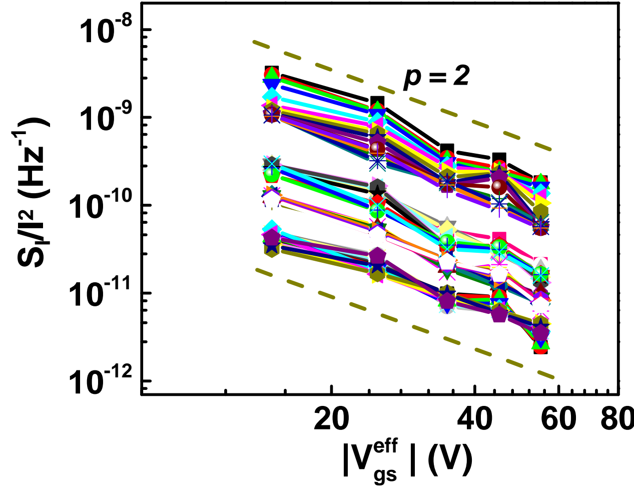

Figure 3.13: Gate voltage dependence of relative noise spectrum ($S(f)$), at different frequencies, for a p-type PVDF-P3HT transistor operating in linear regime. The dashed lines show reference plot corresponding to $p = 2$.

To obtain the value of p, a log-log plot of the normalised PSD ($S(f)$) and effective gate voltage ($1/V_{gs}^{eff}$) is fitted to a linear equation and the slope (or p) obtained from the fit.

$$S(f) \propto \frac{1}{(V_{gs}^{eff})^p} \Rightarrow S(f) = \frac{C_1(constant)}{(V_{gs}^{eff})^p} \tag{3.2}$$

$$log(S(f)) = -p.log(V_{gs}^{eff}) + log(C_1) \tag{3.3}$$

From fig-3.13, it is observed that slope (p) is close to 2 (2 ± 0.2)

Time series plots

The time series (current) data from these measurements are plotted as histograms to obtain the amplitude distribution of the sampled signals. The plotting parameters have been kept constant in all the plots, and are mentioned below:

- Number of bins for histogram plot : 35
- Number of data points for each plot : 50,000
- Range of current amplitude : -0.15 to 0.15 nA
- Number of counts shown in Y-axis (common for all plots) : 8400

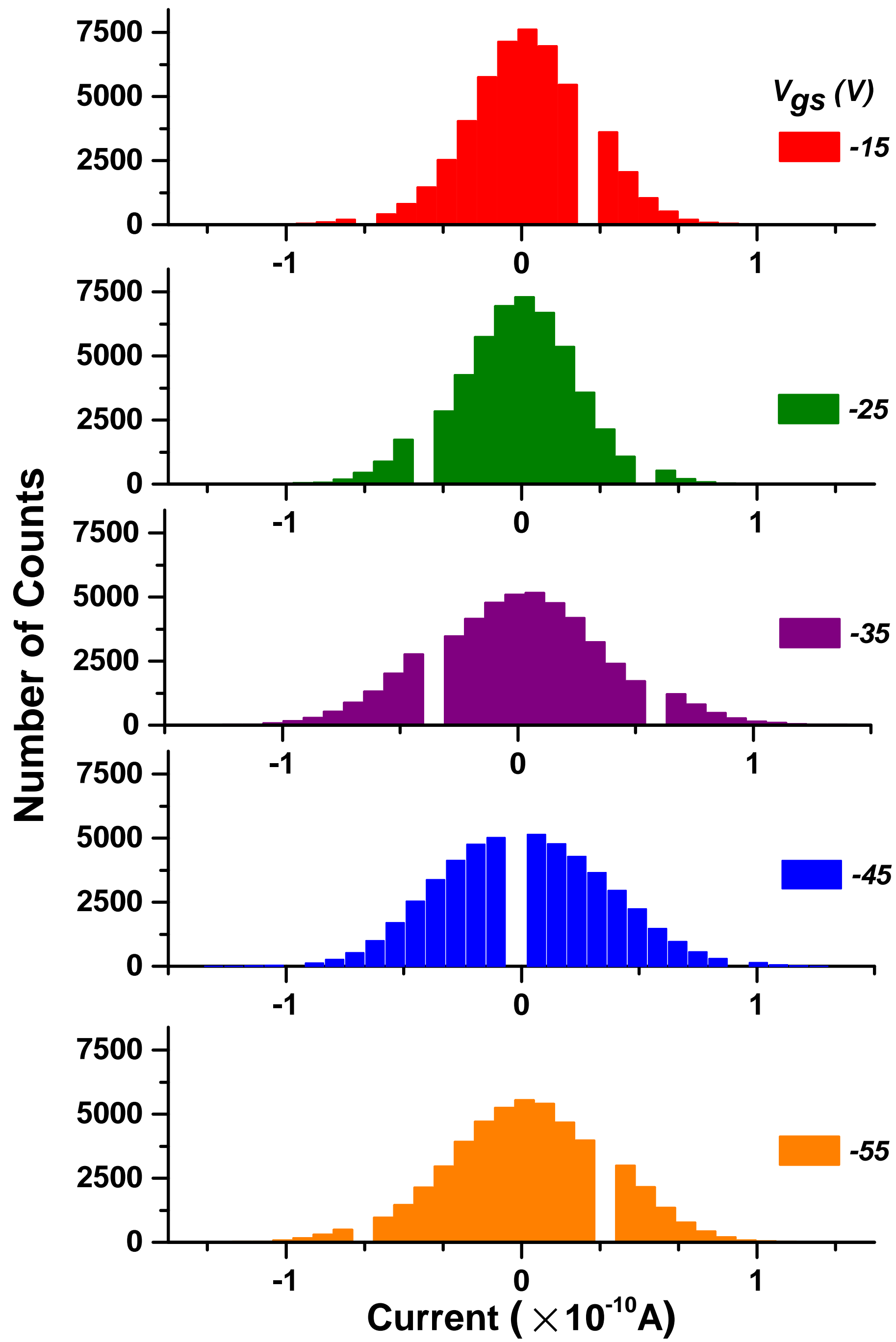

Figure 3.14: Histogram plots for time series data for a p-type transistor operating in linear regime, obtained at different gate bias and constant drain bias (-10V).

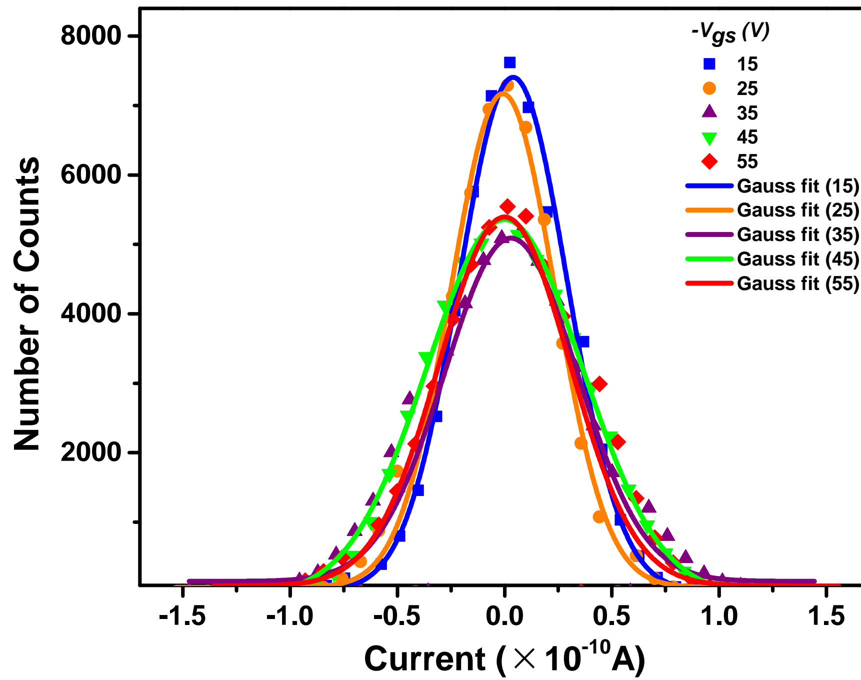

Figure 3.15: Gaussian fitting of the histogram plots (fig-3.14) obtained at different gate bias for a p-type transistor, operating in linear regime.

The amplitude distribution of histogram plots, at different V_{gs}, are plotted in a single graph window and fitted with gaussian curve as shown in fig-3.15.

Saturation regime

In this study, PP transistor is biased in saturation regime where $V_{ds} > V_{gs}^{eff}$ and the channel current noise is measured at different gate voltage. The DC characteristics are shown in fig-3.7 and 3.8.

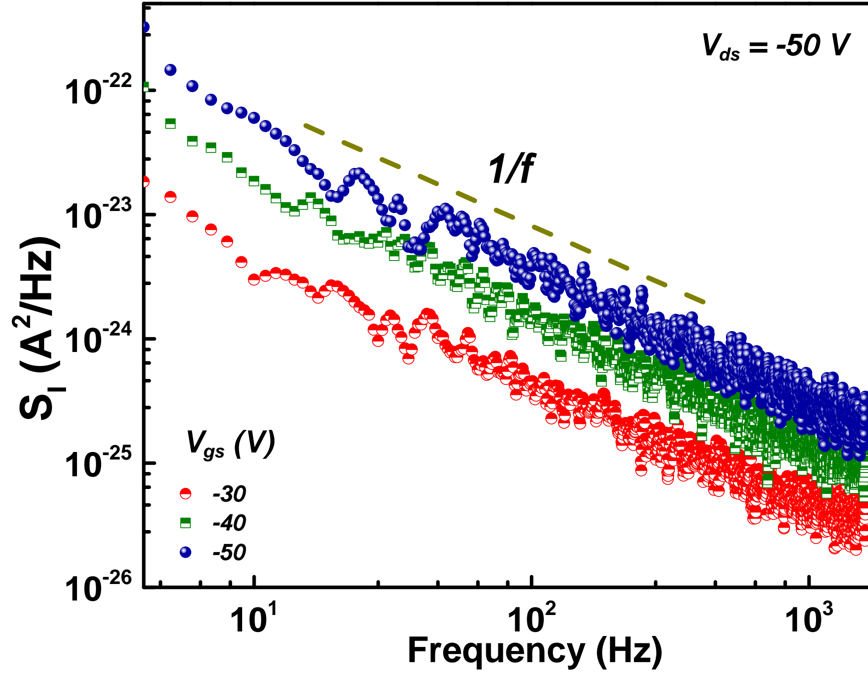

Figure 3.16: Current noise spectrum ($S_I(f)$) plotted as a function of frequency, in saturation regime, at different gate bias and constant drain bias (-50 V) for a p-type PVDF-P3HT transistor (fig-3.7). The dashed line shows a reference 1/f plot.

The PSD is measured at different gate bias[e] while keeping V_{ds} constant (-50 V). The corresponding noise spectrum (fig.3.16) exhibits a $1/f^{\alpha}$ type behaviour with α close to 1 (1 ± 0.1). The I-V characteristics change for saturation regime as compared to linear regime. The exponent p, in this case, is obtained from the relation $(S_I(f)) \propto (V_{gs}^{eff})^p$). This equation can also be written as, $log(S_I(f)) = p.log(V_{gs}^{eff}) + log(C_2)$.

[e] $V_{gs}(V) \in [-30, -34, -40, -44, -50]$

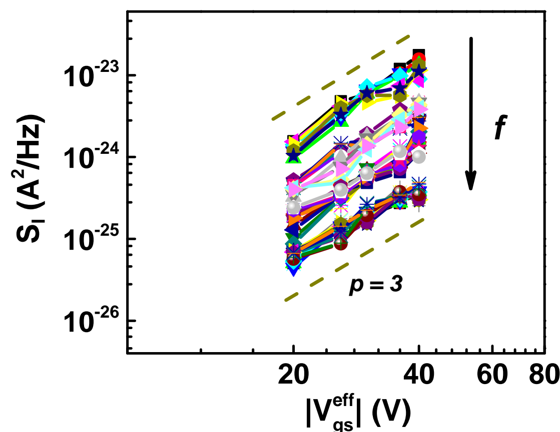

Figure 3.17: Gate bias dependence of power spectrum (fig-3.16), in saturation regime, for a p-type PVDF-P3HT transistor. The dashed lines show reference plots corresponding to p =3

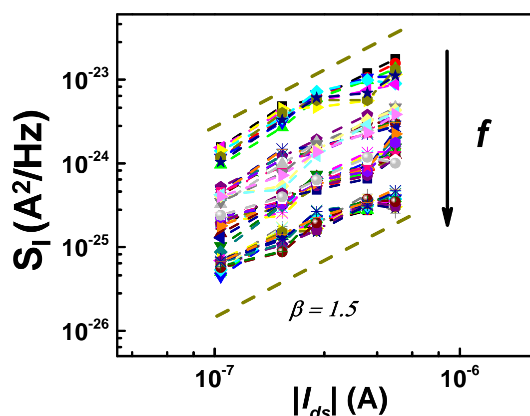

Figure 3.18: Source-drain current dependence of power spectrum (fig-3.16), in saturation regime, for a p-type PVDF-P3HT transistor. The dashed lines show reference plots corresponding to β =1.5

The gate dependence (p) of the PSD is obtained by experimental curve fitting to the log-log plot of $S_I(f)$ versus V_{gs}^{eff}. In this study, value of p lies close to 3 (fig.3.17). Since $I_{ds} \propto (V_{gs}^{eff})^2$, current exponent β is expected to take a value of $p/2$ and is observed (fig.3.18).

Time series plots

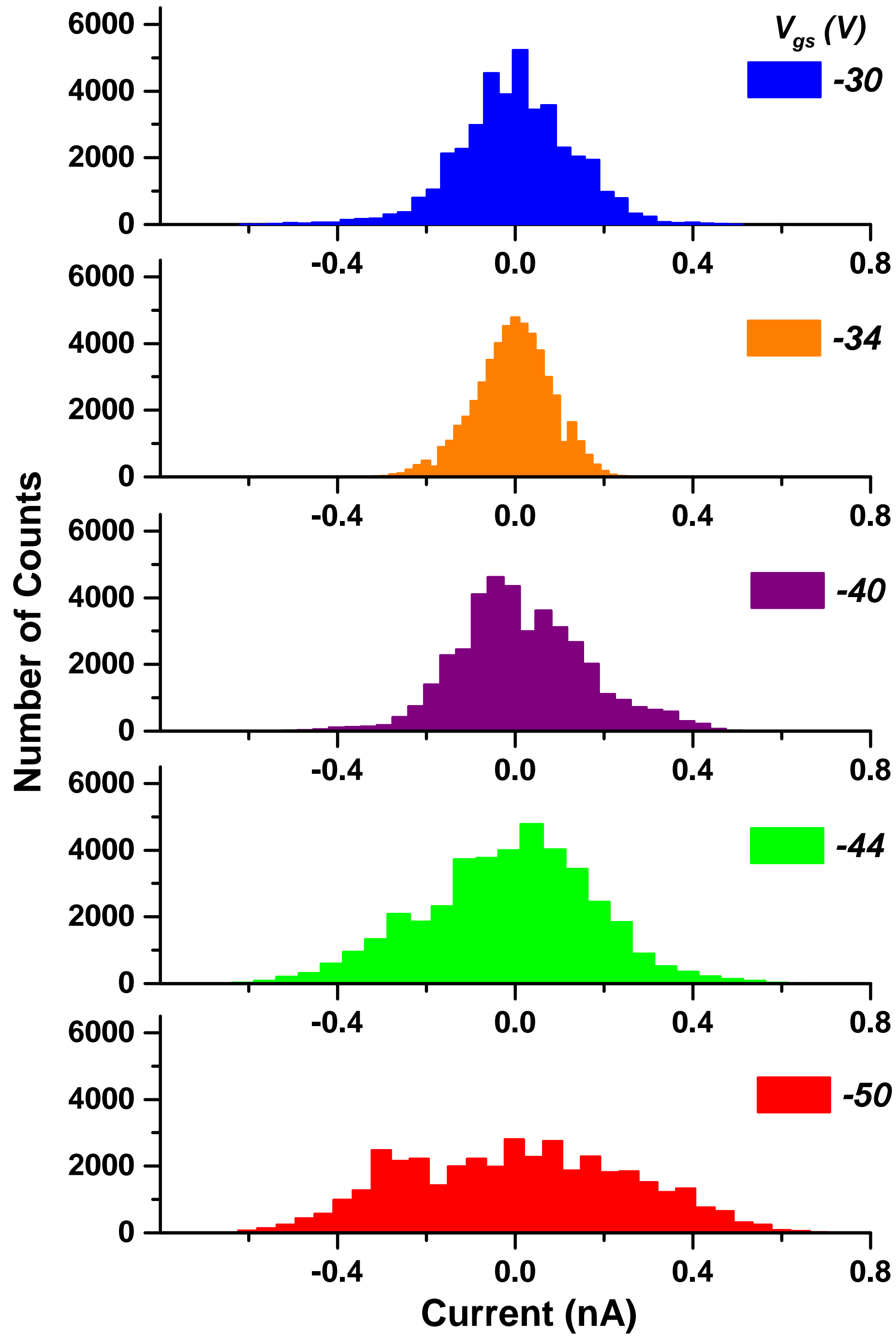

Figure 3.19: Histogram plots for time series data for a p-type transistor operating in saturation regime, obtained at different gate bias and a constant V_{ds} (-50V).

The time series data is plotted as histogram (fig-3.19), similar to that in linear regime. For plotting histogram, the parameters have been kept constant, and are mentioned below:

- Number of bins for histogram plot : 35
- Number of data points for each plot : 40,000
- Range of current amplitude : -0.78 to $0.84\ nA$
- Number of counts shown in Y-axis (common for all plots) : 6400

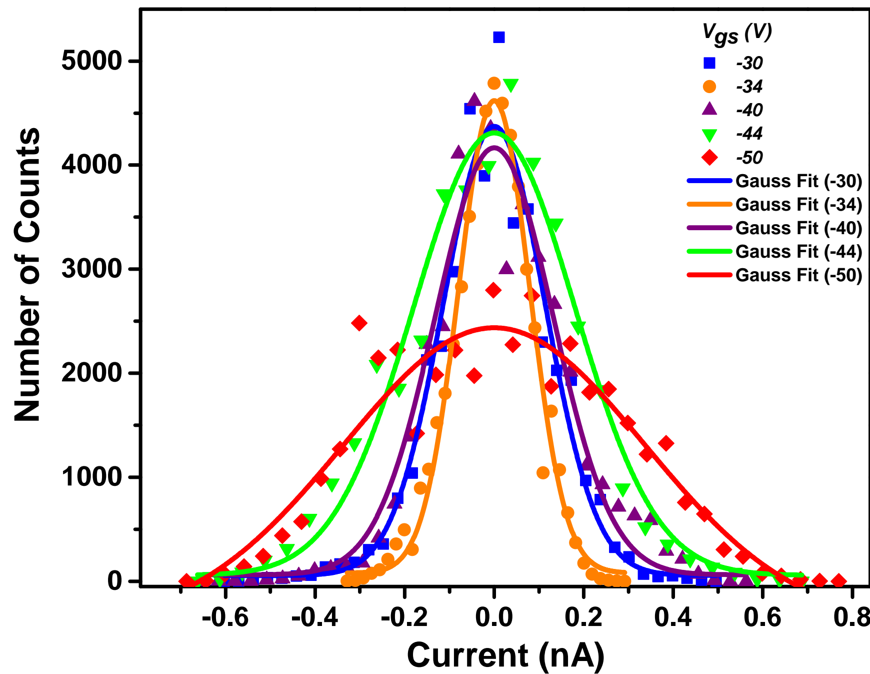

Figure 3.20: Gaussian fitting of the histogram plots (fig-3.19) obtained at different gate bias for a p-type transistor operating in saturation regime.

The amplitude distribution of the time series data obtained from fig-3.19 is fitted to gaussian distribution and is depicted in fig-3.20.

3.1.4 Leakage gate current noise

This section is dedicated to the study of leakage gate current noise ($S_{I_{gs}}(f)$) in PP transistors. The transistors used in this section show stable DC characteristics, marked by distinct linear and saturation regimes, similar to fig-3.7 and fig-3.8. To measure noise in gate current (I_{gs}), the drain terminal is kept float (open circuit) and the corresponding current measured in gate-source circuit.

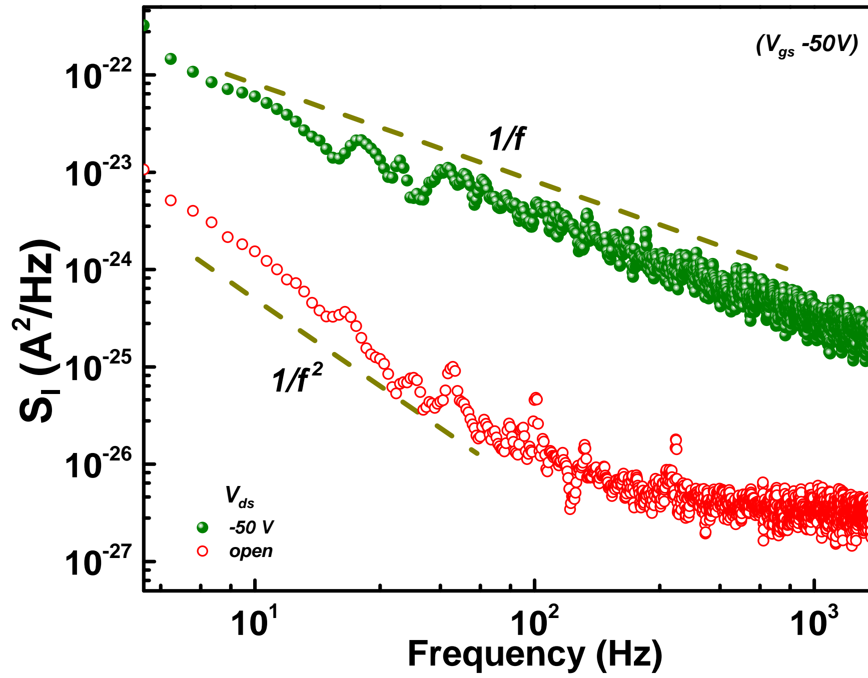

Figure 3.21: Comparison between gate and source-drain current noise at a constant gate bias (-50V) for a p-type transistor (PVDF-P3HT). Reference $1/f^{\alpha}$ slopes are shown for α =1 and 2, in dashed lines.

The magnitude of $S_{I_{gs}}(f)$ is compared with channel current noise ($S_I(f)$), for low leakage transistors, and shown in fig-3.21. In this measurement, V_{gs} is kept constant at -50 V while V_{ds} is at -50 V (for $S_I(f)$) and open circuit (for $S_{I_{gs}}(f)$). Corresponding current values are 590 nA (I_{ds}) and 30 nA (I_{gs}). From the PSD plots, it is observed that gate and channel current noise take different values of slope or the frequency exponent α (from eqn.1.16). $S_{I_{gs}}(f)$ is characterized by an α value close to 2 ($f < 100$ Hz) while for $S_I(f)$, $\alpha \sim 1$.

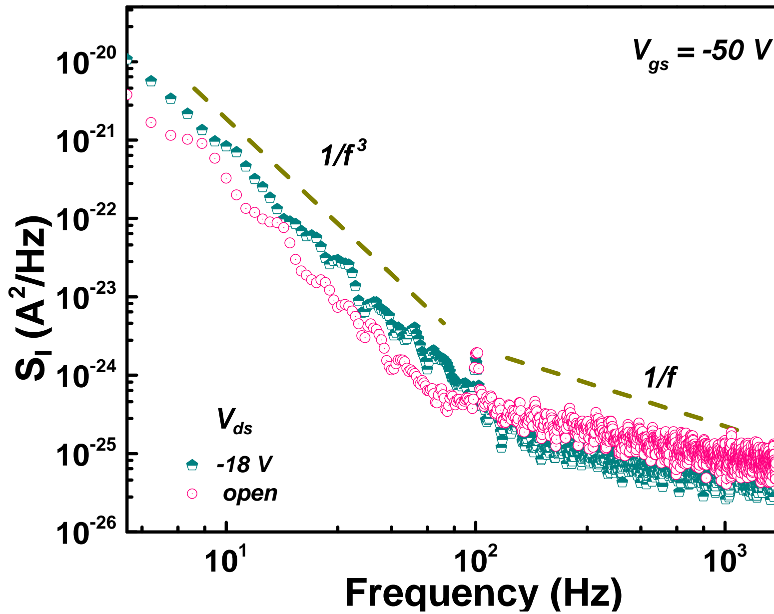

Figure 3.22: Current noise spectra of gate and source-drain current shown for a high leakage p-type transistor (PVDF-P3HT), at constant gate bias ($V_{gs} = -50V$). Reference $1/f^{\alpha}$ slopes are shown for α =1 and 3, in dashed lines.

Similarly, the noise spectra are compared for a PP transistor having higher gate leakage, and depicted in fig-3.22. For this measurement, V_{gs} is kept constant at -50 V while V_{ds} is at -18 V (for $S_I(f)$) and open circuit (for $S_{I_{gs}}(f)$). Corresponding current values are 670 nA (I_{ds})and 340 nA (I_{gs}). Thus, gate current magnitude is almost 50% of the SD current. The noise amplitude for channel and gate current noise (fig-3.22) are almost equal and have similar shape.

The measurement were carried out at other V_{ds} values (in the same device) as well (-8 V to -18 V, in steps of -2 V). In all of these measurements, magnitude of $S_{I_{gs}}(f)$ is found comparable to $S_I(f)$, as seen in fig-3.22. From the PSD plots, it is observed that noise spectrum has two distinct regions characterized by different slope values. A clear "corner" frequency can be seen at $\sim$ 100 Hz where the slope changes.

The higher value of α ($\sim$ 2) is typical of $S_{I_{gs}}(f)$ while α is close to unity for $S_I(f)$ (as observed in fig-3.21). The α value in the noise spectrum, for high leakage transistor, is referred to as gate-exponent "α_g", for $f < 100$ Hz, while the exponent corresponding to $f > 100$ Hz, is termed as "α_{ch}".

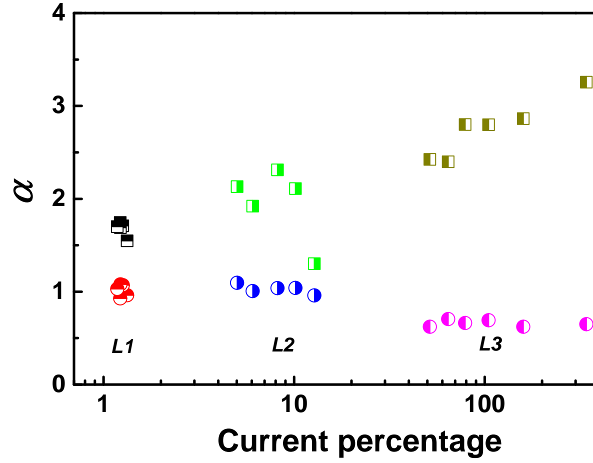

Figure 3.23: Frequency exponent, α (from Hooge relation), in the noise spectra of gate and channel current is plotted as a function of leakage current percentage ($C.P.$), for three devices-L1, L2 and L3 (p-type transistors based on PVDF-P3HT). Square shaped data points denote gate-exponent (α_g) while circles represent channel exponent α_{ch}.

The frequency exponents, α_g and α_{ch} were obtained for three PP transistors which showed varying levels of leakage gate current. The devices in this study are referred to as L1, L2 and L3. In fig-3.23, circles represent α_{ch} while square represent α_g. The exponents are plotted as a function of current percentage ($C.P.$) in this figure, where $C.P.$ is defined as

$$C.P. = \left(\frac{I_{gs}}{I_{ds}}\right) \times 100 \tag{3.4}$$

The PSD plots for device L2 and L3 that showed C.P. of $\sim$ 5 % and $\sim$ 50 % are shown in fig-3.21 and 3.22, respectively. The leakage in device L1 is quite less ($\sim$ 1%). Each data point in this plot corresponds to a given set of measurement, and is described below:

- *L1:* $V_{gs}(V) \in [-30, -40, -50, -60, -70]$; V_{ds} at -30 V and float.
- *L2:* $V_{gs}(V) \in [-30, -34, -40, -44, -50]$; V_{ds} at -50 V and float.
- *L3:* $V_{ds}(V) \in [-8, -10, -14, -16, -18]$ and float; V_{gs} at -50 V.

From the plot of α versus $C.P.$, it is clearly seen that the α_g increases (1.7 - 3.5) with gate leakage current while α_{ch} remains close to unity (0.7 - 1.1).

3.1.5 Effect of light

The effect of photo-illumination on current noise of PP transistors is studied in this section. A continuous beam helium-neon (He-Ne) laser of wavelength 543 nm and power output of 2 mW has been used to excite charge carriers in the semiconductor (P3HT). Light experiments have been performed on transistor biased in depletion mode. To operate p-type OFET in depletion mode, the gate bias is kept at positive polarity whereas for accumulation, polarity is negative. In depletion mode, the dielectric-semiconductor interface of a p-type OFET provides large resistance for hole conduction and the transport is mostly through the bulk of semiconductor.[79]

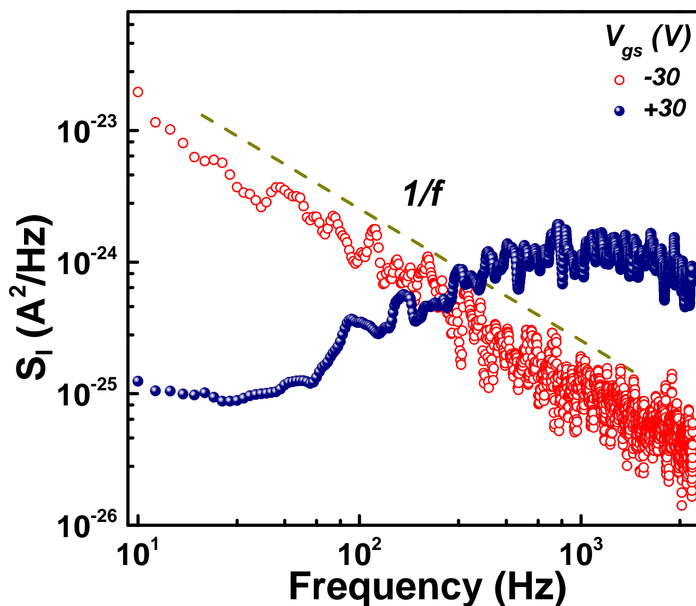

Figure 3.24: Noise spectrum of source-drain current for a p-type (PVDF-P3HT) transistor operated in accumulation and depletion mode, at constant V_{ds} (-50V). The dashed line shows reference 1/f slope.

The DC characteristics (accumulation mode) of the PP transistor, used for light studies in this section, are similar to that shown in fig.3.7 and 3.8. The threshold voltage for this transistor is 10 V. The SD current output for different set of bias conditions are mentioned below:

- *Accumulation mode* $V_{ds} = -50V$, $V_{gs} = -30V$ and $I_{ds} = -253nA$
- *Depletion mode* $V_{ds} = -50V$, $V_{gs} = +30V$ and $I_{ds} = -14nA$

The trans-impedance gain for noise measurement has been kept at 10^7 V/A to amplify the current fluctuations and to maintain a frequency bandwidth of 50 kHz[f]. The current noise spectrum corresponding to the accumulation and depletion mode (in dark conditions) is compared in fig.3.24. The spectral features of current noise are quite different in these modes. In the depletion mode, a wide peak at 1 kHz is observed while in accumulation mode, noise spectrum has a typical $1/f^{\alpha}$ type feature ($\alpha \sim 1.05$).

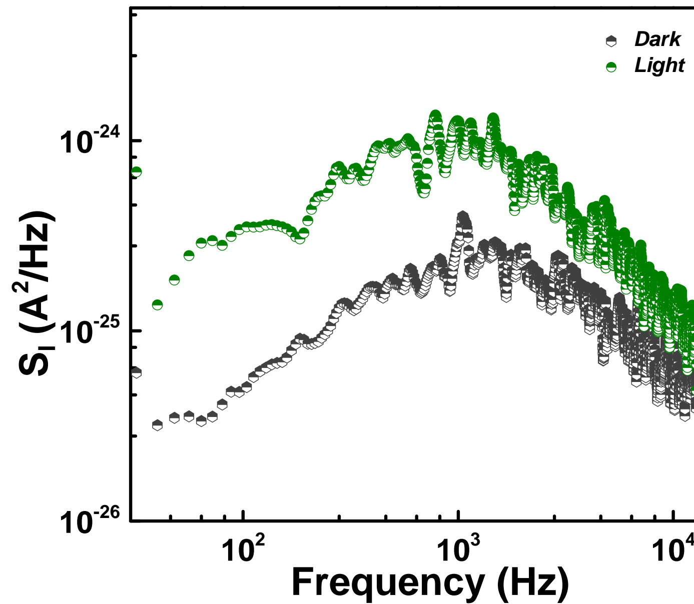

Figure 3.25: Current noise spectrum in dark and light conditions for a p-type transistor (PVDF-P3HT) operated in depletion mode for $V_{gs} = 30V$ and $V_{ds} = -50V$

The noise spectrum (in depletion mode) corresponding to light and dark conditions are depicted in fig-3.25. The experiment details for this measurement are summarized below:

- $V_{gs} = +30V$ and $V_{ds} = -50V$
- In dark condition, SD current $I_d = 14nA$ while in light $I_{ph} = 27nA$
- Measured frequency range: 8 Hz to 12.8 kHz.
- Time duration for one data frame: 125 milliseconds

[f] *Source:* Femto DLPCA-200 datasheet

- Number of data-frames in one data set: 20
- Time duration of laser irradiation for one data set: ~ 5 seconds
- Time duration between successive laser experiments: > 10 minutes

The channel area can be assumed to uniformly illuminated since the FWHM of laser beam intensity or spot diameter is > 2 mm while the device has a channel length of 26 microns and a width of 0.96 mm. Upon light illumination, the current magnitude increases and the percentage change, ΔI is given by

$$\Delta I = \left(\frac{I_{ph} - I_d}{I_d} \right) \times 100 \approx 92\% \tag{3.5}$$

This increase in noise amplitude is observed with the maximum intensity of laser irradiation. Intensity dependent studies were difficult due to the small changes in noise spectrum. Increasing gain could circumvent these problems but the bandwidth of the measurement would be compromised, which is undesirable since the power spectrum spans over a wide range of frequency.

3.2 Discussions

The results obtained from noise measurements on n-type and p-type OFETs are discussed in this section. The PSD analysis of current fluctuations is based on Hooge's empirical relation (eqn-1.18) and the parameters within.

BCB-N2200 transistors

It was observed that the DC characteristics (fig-3.1 and 3.2) of a n-type BN transistor, do not truly represent the behaviour of a stable and working transistor. A gate dependence was seen in the output channel current and the current fluctuations were measured at various V_{gs} values (keeping V_{ds} constant). The noise spectrum showed a $1/f^{\alpha}$ type behaviour with $\alpha \sim 1.4$. However, the current characteristics changed significantly during the noise measurement. The measured current fluctuations, thus, have a transient character in the mean current value. Noise spectrum, usually analysed by the hooge equation (eqn.1.18) is inadequate to quantitatively

analyse such behaviour. It is applicable only for current fluctuations that are present over a constant DC current.[29]

The channel current of BN transistors shows a $1/f^{\alpha}$ type behaviour but its difficult to find the source of noise, except that it has a gate dependence. The origin of noise has been a complex issue since a large number of factors (collectively or individually) can manifest as flicker noise spectrum.[23] It has been known that n-type PFETs are susceptible to oxygen and moisture that introduces interfacial trap states within HOMO-LUMO energy levels[51] affecting the charge transport. Apart from oxygen/moisture induced traps, various other factors may as well contribute to device performance. For BN transistors, further noise analysis was not possible due to the instability in static characteristics. The transistor stability in terms of DC characteristics, thus, is a necessary condition for reliable noise analysis.

BCB-P3HT transistors

The p-type BP transistors showed distinct linear and saturation regime (fig-3.4) with relatively less drift in channel current, as compared to BN transistors. The current magnitude remained almost constant before and after the noise measurement for such devices. The current noise (fig-3.6) was measured in linear (or ohmic) regime of transistor at different V_{ds} (V_{gs} was kept constant). In this study, the free charge carrier density N remains constant for this study since N is proportional to V_{gs}. The observed PSD, at various V_{ds}, showed a $1/f^{\alpha}$ type behaviour ($\alpha \sim 1.4$) but the noise magnitudes were similar for different values of I_{ds} (or V_{ds}). According to Hooge's equation (eqn.1.16), the noise amplitude ($S_I(f)$) increases with the current bias (I) (provided N remains constant). For metallic samples, silicon MOSFET and even in organic thin film transistors, it is usually observed that $S_I(f) \propto I^2$. The current exponent β typically lies in the range 1 - 2 depending on the material and/or the source of noise.[30]

While these PFETs showed stable DC characteristics, the noise properties were still difficult to explain. The current independent behaviour of PSD suggests that other noise source dominates the channel noise spectrum, for example, contact resistance at metal-semiconductor interface.[80] Measurements on other BP transistors showed similar results in the noise spectrum. This suggests that transistor stability,

in terms of DC characteristics, is a necessary but not a sufficient condition for noise analysis.

PVDF-P3HT transistors

The p-type PP transistors showed very less drift in transistor characteristics. They were analysed in different operating regimes and bias conditions.

Drain voltage dependence

At constant V_{gs}, the noise spectrum showed current (V_{ds}) dependence with $\beta \sim 0.9$ (fig-3.11). The current exponent, β is usually associated with the source of noise[30] in the material. According to hooge model, its value is 2 and represents bulk conductivity fluctuations in the solid. However, β deviates from the proposed constant value (two) for current noise in transistors. It has been observed that β lies between 1.5 - 2 for channel current noise in transistors.[41] Smaller β values, in case of PP transistors, suggests that noise sources have an interface origin (surface phenomena). The dielectric-semiconductor interface can be assumed to be the origin of conductivity fluctuations.

In the linear regime, transistor is modelled as an ohmic resistor. However, β is different for ohmic transport in organic semiconductor (≈ 1) and in metals (≈ 2). Noise being a reflection of charge transport in a material suggests that fundamental mechanism of carrier transport is different in organic semiconductor and metals, even when DC characteristics are same.

Gate voltage dependence

The gate voltage is related to the number of free charge carriers N at the channel interface by eqn.1.13. The power spectrum can be expressed as,

$$S(f) = \frac{S_I(f)}{I^2} \propto \frac{1}{(V_{gs}^{eff})^p}$$

Here, the exponent p is used to identify the noise model that explains the observed noise spectrum.

The noise studies were performed both in linear and saturation regime of transistor operation at various gate voltages (keeping V_{ds} constant). In the ***linear regime***, the relative PSD ($S(f) = S_I(f)/I^2$) showed a 1/f behaviour with $\alpha \sim 1$ (fig.3.12). The gate voltage dependence of $S(f)$ is obtained from fig-3.13 and it can be seen that p is very close to 2. A value of $p = 2$ is indicative of McWhorter's number density fluctuation (eqn-1.25) for observed noise spectrum, in MOSFETs. McWhorter model for carrier density fluctuation[25,34,35,47] is concerned with the tunnelling of electrons in the (oxide based) gate dielectric which cannot be applied to PFETs, since the dielectric is a polymer and holes are the majority charge carriers in the channel current. However, it is possible that trapping-detrapping of charges takes place due to surface trap states at the dielectric-semiconductor interface and finally result in number density fluctuations. In that case, the assumption of oxide dielectric is to be replaced with a more appropriate explanation supported by mathematical equations.

In the ***saturation regime***, the PSD showed a $1/f^\alpha$ type behaviour with $\alpha \sim 1$ (fig.3.16) and a gate voltage dependence identified by exponent p (fig-**??**). The experimental fit to curve in fig-3.17 gives $p \approx 3$ which suggests Hooge mobility fluctuation model (eqn-1.15). Since $I_{ds} \propto (V_{gs}^{eff})^2$, current exponent β is expected to take a value of $p/2$ which is indeed observed in fig-3.18. The general consensus, regarding noise models, is that both number and mobility fluctuation sources are present in the system and either can dominate the total noise spectrum.[40] It is also possible that sometimes both sources may have significant contributions.[26] The current noise fits to number density fluctuation model for linear regime studies and to mobility fluctuation model for saturation regime studies.

The strength of applied electric field along the channel (drain-source voltage), is different in the two studies. Measurements have been carried out at low drain bias ($-10V$) in linear regime, and at high bias ($-50V$) in saturation regime. With high electric field , the charge carriers are constrained to move in a preferred direction which could lead to more scattering events. It is usually observed that mobility fluctuations dominate when the density of free charge carriers is larger than the density of traps, limiting the contribution of number density fluctuations.[26,36] Thus, for high electric fields in OSCs, mobility fluctuations may dominate in the noise spectrum because of higher density of carriers, in a given direction, compared to the

trap states. Following similar reasoning, it can be argued that at low electric fields, the number density fluctuation dominates the total noise spectrum.

For mobility fluctuations or the hooge model, the hooge's constant γ_H can be calculated from the following relation,

$$\gamma_H = \frac{S_I(f) \times f \times N}{I^2} \tag{3.6}$$

The calculations have been done for all the data points at $f = 10Hz$ (fig-3.16), value of N is obtained using eqn.1.13 and $C_i = 28\ nFcm^{-2}$ for the PP transistor. In saturation regime, the value of $\gamma_H \approx 4.1$ (4.1 ± 0.1) which is consistent with other reports on OFETs[57,66,68] and is slightly higher than crystalline MOSFETs.[81] For other models, γ_H is dependent on the current magnitude and the frequency, and is no longer a constant. In the linear regime, γ_H lies in the range $\sim 4 - 50$. The magnitude of hooge constant is an indication of relative noise present in the system. It is useful for comparing system performance which obeys hooge model.

Leakage gate current noise

Ideally, the gate-source current (I_{gs}) should be negligible ($\sim 10^{-11} - 10^{-12}A$), and is mostly the case with crystalline MOSFETs. However, in PFETs, it has been observed that I_{gs} levels are relatively higher ($\sim 10^{-9} - 10^{-10}A$) and may increase with time.

The reliability of OFETs is one of the major issues and a bottleneck for commercial applications. The leakage gate current often increases with operation time and the reason is mainly attributed to bias stress, ionic transport or electrode migration.[51] It is induced in the polymer material due to their low tolerance towards electric field. As a consequence of bias stress, the gate dielectric behaves like a lossy capacitor with increased conductivity, and subsequently affects the device performance. A high leakage gate current in a transistor may lead to an increased power consumption affecting the working of otherwise working transistors, in an integrated circuit environment.

The total noise in output SD current of a transistor is a combination of gate current noise ($S_{I_{gs}}(f)$) and the channel noise ($S_{I_{ds}}(f)$ or $S_I(f)$). These noise sources have spatially different origin and so they can be assumed to uncorrelated. The total

noise then becomes the addition of these two sources. In the present noise studies, a portion of $S_{I_{gs}}(f)$ is present but because of its relatively low magnitude, overall spectrum is dominated by $S_I(f)$, as shown in fig.3.21. A clear distinction can be seen between the spectrum of I_{gs} and I_{ds} in the form of different slope values, in the measured frequency range. The former is characterized by $\alpha \sim 2$ while the latter shows a typical $1/f^{\alpha}$ type behaviour with $\alpha \sim 1$. In case of stable and working transistors with low leakage, I_{gs} magnitude is quite less compared to I_{ds} and so the total output noise is dominated by conductivity fluctuations at the interface.

The noise spectrum of gate current, which has a higher slope at low frequencies, is expected to dominate the channel noise if the current levels (I_{gs}) are high enough, as shown in fig-3.22. The total noise spectrum in this case has significant contribution from both gate and SD current, and a clear cross-over is observed at $\sim$ 100 Hz. In this case, the channel noise departs from the ideal 1/f type form and is dominated by the $1/f^3$ behaviour of gate current noise. The higher α value is related with $S_{I_{gs}}(f)$ and is referred as gate-exponent "α_g" and exponent "α_{ch}" to channel noise.

From fig.3.21 and 3.22, it is observed that $S_{I_{gs}}(f)$ dominates at $f < 100$ Hz (low leakage) and a crossover is seen in the $S_I(f)$ for high leakage devices. The frequency exponents in PSD plots, measured for three devices, are plotted in fig.3.23 which show that α_g increases $(1.7-3.5)$ with relative percentage of leakage current $(C.P.)$ while α_{ch} remains fairly constant $(0.7-1.1)$. The gradual increase in leakage current is not readily observed in the FET characteristics, but is quite obvious in the PSD evolvement. Such spectral features in channel current noise serve as a useful tool to monitor device degradation.

Effect of light

The effects of photo-illumination on current noise were studied in the depletion mode of transistor operation. In depletion mode, the polarity of gate bias in OFETs is such that the majority charge carriers are repelled from the interface, and encountered by a greater resistance path which decreases the channel current. The conduction between the SD electrodes then takes place through the bulk of the semiconductor, away from the depletion region.[79]

The fluctuations in I_{ds} in accumulation mode (negative V_{gs}) has a typical $1/f^{\alpha}$ type spectrum while current in depletion mode shows a wide peak in the power

spectrum (fig-3.24) around 1 kHz, in range $\sim$ 10 Hz to 10 kHz. The spectral features of drain current, in depletion mode, is indicative of transport through the bulk of semiconductor. This particular feature of having a peak at some frequency (1 kHz, here), is representative of generation-recombination (g-r) type noise observed in organic semiconductors.[82]

The I_{ds} noise spectrum, in depletion mode and in dark conditions, show features that can be correlated with bulk conductivity fluctuations. Light illumination on semiconductor (P3HT) leads to excitation of charge carriers in the volume (or bulk)[(g)]of the sample. The effect of light can be viewed simplistically as an equivalent to a greater gate bias, with an enhanced value of I_{ds} (referred as I_{ph}). The percentage increase in current (light and dark conditions) is almost 90% for the measured device (fig-3.25). Measurements on (three) other devices showed ΔI as high as 500 % however the absolute current magnitude were in the range of few pico-amperes and the corresponding noise was dominated by the thermal noise.

A comparison of noise spectra (fig-3.25) in light and dark conditions suggests that the noise mechanisms are identical. The shape of noise spectrum (in dark) is retained upon light illumination along with the a wide g-r type feature having center frequency at 1 kHz, and only the magnitude is seen to increase. The magnitude of spectrum is a manifestation of the number of transition events (or fluctuations) of carriers that contribute to total noise. Thus, the influence of light has been to amplify the events taking place in dark conditions (bulk conductivity fluctuations). The generation-recombination of charges can be correlated with holes participating in the trapping-detrapping events between the bulk of semiconductor and the depletion region near the interface. The centre frequency (at 1 kHz)and g-r noise feature were consistent with noise measurements on (five) other devices.

[(g)]the thickness of P3hT film is $\sim 50\ nm$.

3.3 Summary

In this thesis, current noise of p-type and n-type PFETs have been studied. Solution processable polymer dielectric (BCB and PVDF) and semiconductor (N2200 and P3HT) were used for the fabrication of PFETs. The current fluctuations from the transistors were amplified, and sampled by a signal analyser for calculating noise. The noise studies in n-type PFETs (BN transistors), were limited since the static (or DC) characteristics changed rapidly during the measurement. The source-drain current noise exhibited a $1/f^{\alpha}$ type behaviour ($\alpha \sim 1.4$) and the noise magnitude was seen to increase with the current bias. In case of p-type BP transistors, the current noise had no dependence with applied drain bias even though the DC characteristics showed improved stability as compared to the n-type transistors. The spectrum, in this case also, had a $1/f^{\alpha}$ type ($\alpha \sim 1.4$) behaviour.

The DC characteristics of p-type PP transistors showed distinct linear and saturation regimes and the devices were stable for longer operation times. Noise studies at fixed V_{gs} showed that the noise spectrum has $1/f^{\alpha}$ type behaviour and takes a linear dependence ($S_I(f) \propto I$) with current value, unlike metallic samples having a square dependence. The current exponent in the power spectrum served useful in identifying the nature of the noise source.

Current noise spectrum, in linear and saturation regime, exhibited 1/f-type behaviour in measured frequency range 1 Hz -1.6 kHz. The observed noise spectrum showed a gate voltage dependence which suggests that the channel current is the dominant noise source. The specific nature of gate dependence has been, traditionally, used to identify the model that explains the mechanism of noise or the conductivity fluctuations in transistors. The linear regime data fitted to the number density fluctuation (or McWhorter) model while the saturation regime data fitted to mobility fluctuation (or Hooge) model. Measurements were carried out at low drain bias ($-10V$) in linear regime, and at high bias ($-50V$) in saturation regime. In both the regimes, the main source of conductivity fluctuations is attributed the interface trap states that lead to either mobility or number density fluctuation.

Noise study on various working devices with varying levels of leakage gate current showed characteristic trend in the power spectra of the channel current noise. The frequency exponent for channel current was found to be close to unity when gate

leakage was less. A relative increase in the gate current, was identified with a higher exponent on frequency term (> 3) in the PSD plot, observed at lower frequencies. The exponents corresponding to SD and gate current noise, in a high leakage transistor, have been observed in spectra of channel noise with a clear cross-over around 100 Hz. Such spectral features are helpful in monitoring device stability. The frequency exponents are related to noise from the (polymer) dielectric and served as an indicator of magnitude of leakage current.

In the last study, noise properties of bulk semiconductor were studied by operating transistor in depletion mode, and in dark conditions. The noise spectra, in this case, showed a broad curve having a peak around 1 kHz in frequency range 10 Hz - 10 kHz. Such features have been attributed to noise due to generation-recombination of charge carriers in the material. With light illumination, noise amplitude was observed to increase taking the similar g-r feature. In this case, the g-r events can take place between the charge carriers (holes) at the interface and bulk of the semiconductor. The intrinsic disorder present in the material and/or the thin film structure can influence the bulk noise properties.

The noise output characteristics of OFETs exhibit the universal $1/f^{\alpha}$ type behaviour. The microscopic origin of the noise has contributions from both mobility and carrier number fluctuations in the channel originating from the interfacial trap states. The SD current in OFETs was identified with characteristics features in the frequency domain. For addressing issues related to device degradation and stability, the leakage gate current was studied in several transistors. The contributions from the gate leakage current to the output I_{ds} appears with unique signature in the noise spectrum, in the form of higher exponent values in the low f range (< 100 Hz). It is seen that $\alpha \approx 1$ for leakage-free devices, while for leakage dominated devices $\alpha \approx 3$. These studies in PFETs points out that low frequency noise analysis can be used to study the charge transport in disordered materials (dielectric and semiconductor) and monitor reliability and degradation.

Appendices

Appendix A

Matlab Code

```
%% Details of the Code
% The PSD is computed by taking the time series file and splitting into
% frames of a specific frequency range, which can be different from the
% settings at DSA. This program can change the lower and
% higher frequency ranges, and performs averaging as well.
%% Created at- Molecular Electronics LAB, JNCASR

function DSA_PSD
format long
clear all

%% Initializing all parameters from the measurement settings
fres = input('Enter the frequency resolution: ');
fspan = input('Enter the frequency span
of time capture in DSA(in Hz): ');
sf = fspan*2.56;
T = input('Enter the total duration of time capture: ');
%minf=1/T;               % lowest frequency possible
fl = input('Enter the lower frequency of plot: ');
fu = input('Enter the upper frequency of plot: ');
t = 1/fl;
```

```
Av=  input('Enter the gain at preamplifier: ');

%% Calling the saved text file into MatLAB
data_file = input('Enter the file name of time series capture: ','s');
fid = fopen(data_file,'r');
data= dlmread(data_file);
X= data(:,1);
X=X./(Av);
len_X= length(X);

%% Initialize parameters for obtainig PSD plots
len_T = T*sf;
len_t= t*sf;               %data points required for one PSD plot
nfft = 2.56*(fu/fl);nfft
Navg = len_T/len_t;
x = zeros(len_t,1);
PSD_total = zeros(nfft,1);
psd_x = zeros(nfft,1);
ptr=0;

for i= 1:Navg

    x = X(1+ptr:len_t+ptr,1);
    psd_x = (fft(x,nfft))./(nfft);
    psd_x = abs(psd_x);
    psd_x = (psd_x.^2);
    PSD_total=PSD_total+psd_x;
    ptr= ptr+len_t;

end
freq=0:fl:fu;
PSD_total = PSD_total/Navg;
PSD_total=PSD_total(1:((nfft/2)+1),1);
```

```
PSD_total(2:end-1,1) = PSD_total(2:end-1,1);

PSD_plt=plot(log10(freq),log10(PSD_total(1:((nfft/2.56)+1))));
xlabel('Frequency (Hz)')
title(data_file)
saveas(PSD_plt,sprintf('some file.bmp'))

%% Saving the PSD plot into text file

freq=transpose(freq);
PSD_write=zeros((fu/fl)+1,2);
PSD_write(:,1)= freq(:,1);
PSD_write(:,2)= PSD_total(1:((nfft/2.56)+1),1);
dlmwrite('some file.txt',PSD_write,'precision',16,
'delimiter',',','newline','pc')

fclose all
    end
```

Bibliography

[1] The nobel prize in physics 1956. *Nobelprize.org*.

[2] Yuan Taur and Tak H. Ning. *Fundamentals of Modern VLSI Devices*. Cambridge University Press, 2nd edition, 2013.

[3] Intel core i7-800 and i5-700 desktop processor series datasheet (vol.1 & 2), 2010.

[4] J.S. Pettinato and D. Pillai. Technology decisions to minimize 450-mm wafer size transition risk. *Semiconductor Manufacturing, IEEE Transactions on*, 18(4):501–509, Nov 2005.

[5] Veaceslav Coropceanu, Jrme Cornil, Demetrio A. da Silva Filho, Yoann Olivier, Robert Silbey, and Jean-Luc Bredas. Charge transport in organic semiconductors. *Chemical Reviews*, 107(4):926–952, 2007.

[6] The nobel prize in chemistry 2000. *Nobelprize.org*.

[7] Anna Khler and Heinz Bssler. *Electronic Processes in Organic Semiconductors, An Introduction*. Wiley.

[8] Jean-Luc Bredas, David Beljonne, Veaceslav Coropceanu, and Jrme Cornil. Charge-transfer and energy-transfer processes in pi-conjugated oligomers and polymers: A molecular picture. *Chemical Reviews*, 104(11):4971–5004, 2004.

[9] Nir Tessler, Yevgeni Preezant, Noam Rappaport, and Yohai Roichman. Charge transport in disordered organic materials and its relevance to thin-film devices: A tutorial review. *Advanced Materials*, 21(27):2741–2761, 2009.

[10] Daniel Tobjork and Ronald Osterbacka. Paper electronics. *Advanced Materials*, 23(17):1935–1961, 2011.

[11] S. D. Baranovskii. Theoretical description of charge transport in disordered organic semiconductors. *physica status solidi (b)*, 251(3):487–525, 2014.

[12] P. M. Borsenberger, L. Pautmeier, and H. Bassler. Charge transport in disordered molecular solids. *The Journal of Chemical Physics*, 94(8):5447–5454, 1991.

[13] H. Bassler. Charge transport in disordered organic photoconductors a monte carlo simulation study. *physica status solidi (b)*, 175(1):15–56, 1993.

[14] Jens Lorrmann, Manuel Ruf, David Vocke, Vladimir Dyakonov, and Carsten Deibel. Distribution of charge carrier transport properties in organic semiconductors with gaussian disorder. *Journal of Applied Physics*, 115(18):–, 2014.

[15] Chengliang Wang, Huanli Dong, Wenping Hu, Yunqi Liu, and Daoben Zhu. Semiconducting pi-conjugated systems in field-effect transistors: A material odyssey of organic electronics. *Chemical Reviews*, 112(4):2208–2267, 2012.

[16] F. Jansson, A.V. Nenashev, S.D. Baranovskii, F. Gebhard, and R. sterbacka. Effect of electric field on diffusion in disordered materials. *Annalen der Physik*, 18(12):856–862, 2009.

[17] I. I. Fishchuk, A. Kadashchuk, S. T. Hoffmann, S. Athanasopoulos, J. Genoe, H. Bssler, and A. Khler. Analytic model of hopping transport in organic semiconductors including both energetic disorder and polaronic contributions. *AIP Conference Proceedings*, 1610(1):47–52, 2014.

[18] J. L. Bredas, J. P. Calbert, D. A. da Silva Filho, and J. Cornil. Organic semiconductors: A theoretical characterization of the basic parameters governing charge transport. *Proceedings of the National Academy of Sciences*, 99(9):5804–5809, 2002.

[19] Henning Sirringhaus. 25th anniversary article: Organic field-effect transistors: The path beyond amorphous silicon. *Advanced Materials*, 26(9):1319–1335, 2014.

[20] Ashu K. Bansal, Shuoben Hou, Olena Kulyk, Eric M. Bowman, and Ifor D. W. Samuel. Wearable organic optoelectronic sensors for medicine. *Advanced Materials*, 2014.

[21] H. Sirringhaus. Device physics of solution-processed organic field-effect transistors. *Advanced Materials*, 17(20):2411–2425, 2005.

[22] Jana Zaumseil and Henning Sirringhaus. Electron and ambipolar transport in organic field-effect transistors. *Chemical Reviews*, 107(4):1296–1323, 2007.

[23] F.N. Hooge. 1/f noise sources. *Electron Devices, IEEE Transactions on*, 41(11):1926–1935, 1994.

[24] A.K. Raychaudhuri. Measurement of 1/f noise and its application in materials science. *Current Opinion in Solid State and Materials Science*, 6(1):67 – 85, 2002.

[25] Hei Wong. Low-frequency noise study in electron devices: review and update. *Microelectronics Reliability*, 43(4):585 – 599, 2003.

[26] E.P. Vandamme and L.K.J. Vandamme. Critical discussion on unified 1/f noise models for mosfets. *Electron Devices, IEEE Transactions on*, 47(11):2146–2152, Nov 2000.

[27] F N Hooge, T G M Kleinpenning, and L K J Vandamme. Experimental studies on 1/f noise. *Reports on Progress in Physics*, 44(5):479, 1981.

[28] F.N. Hooge and L.K.J. Vandamme. Lattice scattering causes 1/f noise. *Physics Letters A*, 66(4):315 – 316, 1978.

[29] P. Dutta and P. Horn. Low-frequency fluctuations in solids: 1/f noise. *Rev. Mod. Phys.*, 53:497–516, Jul 1981.

[30] A. van der Ziel. Unified presentation of 1/f noise in electron devices: fundamental 1/f noise sources. *Proceedings of the IEEE*, 76(3):233–258, Mar 1988.

[31] L.K.J. Vandamme. Noise as a diagnostic tool for quality and reliability of electronic devices. *Electron Devices, IEEE Transactions on*, 41(11):2176–2187, Nov 1994.

[32] F.N. Hooge. On the additivity of generation-recombination spectra. part 1: Conduction band with two centres. *Physica B: Condensed Matter*, 311(34):238 – 249, 2002.

[33] F.N. Hooge. On the additivity of generation-recombination spectra. part 2: 1/f noise. *Physica B: Condensed Matter*, 336(34):236 – 251, 2003.

[34] L.K.J. Vandamme and F.N. Hooge. On the additivity of generation-recombination spectra part 3: The mcwhorter model for 1/f noise in {MOSFETs}. *Physica B: Condensed Matter*, 357(34):507 – 524, 2005.

[35] L.K.J. Vandamme and F.N. Hooge. What do we certainly know about 1/f noise in mosts? *Electron Devices, IEEE Transactions on*, 55(11):3070–3085, Nov 2008.

[36] T. G. M. Kleinpenning and L. K. J. Vandamme. Model for 1/f noise in metal-oxide-semiconductor transistors. *Journal of Applied Physics*, 52(3):1594–1596, 1981.

[37] K.K. Hung, P.K. Ko, Chenming Hu, and Y.C. Cheng. A unified model for the flicker noise in metal-oxide-semiconductor field-effect transistors. *Electron Devices, IEEE Transactions on*, 37(3):654–665, Mar 1990.

[38] A Van der Ziel, PH Handel, Xichen Zhu, and Kuang Hann Duh. A theory of the hooge parameters of solid-state devices. *Electron Devices, IEEE Transactions on*, 32(3):667–671, 1985.

[39] Joseph F. Stephany. Origin of 1/f noise in metallic conductors and semiconductors. *Phys. Rev. B*, 46:12175–12180, Nov 1992.

[40] L.K.J. Vandamme. Bulk and surface 1/f noise. *Electron Devices, IEEE Transactions on*, 36(5):987–992, May 1989.

[41] S. Martin, A. Dodabalapur, Z. Bao, B. Crone, H. E. Katz, W. Li, A. Passner, and J. A. Rogers. Flicker noise properties of organic thin-film transistors. *Journal of Applied Physics*, 87(7):3381–3385, 2000.

[42] D. Rigaud, M. Valenza, and J. Rhayem. Low frequency noise in thin film transistors. *Circuits, Devices and Systems, IEE Proceedings* -, 149(1):75–82, Feb 2002.

[43] G. Giusi, O. Giordano, G. Scandurra, S. Calvi, G. Fortunato, M. Rapisarda, L. Mariucci, and C. Ciofi. Evidence of correlated mobility fluctuations in p-type organic thin film transistors. *Electron Device Letters, IEEE*, PP(99):1–1, 2015.

[44] Alexander A. Balandin. Low-frequency 1/f noise in graphene devices. *Nat Nano*, 8(8):549–555, August 2013.

[45] S.L. Rumyantsev, C. Jiang, R. Samnakay, M.S. Shur, and A.A. Balandin. 1/ f noise characteristics of mos2 thin-film transistors: Comparison of single and multilayer structures. *IEEE Electron Device Letters,*, 36(5):517–519, May 2015.

[46] Oana D. Jurchescu, Behrang H. Hamadani, Hao D. Xiong, Sungkyu K. Park, Sankar Subramanian, Neil M. Zimmerman, John E. Anthony, Thomas N. Jackson, and David J. Gundlach. Correlation between microstructure, electronic properties and flicker noise in organic thin film transistors. *Applied Physics Letters*, 92(13):–, 2008.

[47] L.K.J. Vandamme, X. Li, and D. Rigaud. 1/f noise in mos devices, mobility or number fluctuations? *Electron Devices, IEEE Transactions on*, 41(11):1936–1945, Nov 1994.

[48] Lin Ke, Surani Bin Dolmanan, Lu Shen, Chellappan Vijila, Soo Jin Chua, Rui-Qi Png, Perq-Jon Chia, Lay-Lay Chua, and Peter K-H. Ho. Impact of self-assembled monolayer on low frequency noise of organic thin film transistors. *Applied Physics Letters*, 93(15):–, 2008.

[49] Vadim N. Savvate'ev, Aharon V. Yakimov, Dan Davidov, Roman M. Pogreb, Ronny Neumann, and Yair Avny. Degradation of nonencapsulated polymer-based light-emitting diodes: Noise and morphology. *Applied Physics Letters*, 71(23):3344–3346, 1997.

[50] S. D. Wang, T. Miyadera, T. Minari, Y. Aoyagi, and K. Tsukagoshi. Correlation between grain size and device parameters in pentacene thin film transistors. *Applied Physics Letters*, 93(4):–, 2008.

[51] Henning Sirringhaus. Reliability of organic field-effect transistors. *Advanced Materials*, 21(38-39):3859–3873, 2009.

[52] Jana Zaumseil. P3ht and other polythiophene field-effect transistors. In Sabine Ludwigs, editor, *P3HT Revisited From Molecular Scale to Solar Cell Devices*, volume 265 of *Advances in Polymer Science*, pages 107–137. Springer Berlin Heidelberg, 2014.

[53] C. Barone, F. Romeo, and S. Pagano. Dynamic behaviors of the charge carriers investigated by means of noise spectroscopy. In *Noise and Fluctuations (ICNF), 2013 22nd International Conference on*, pages 1–4, June 2013.

[54] H. Katsu, Yoshitaka Kawasugi, R. Yamada, and Hirokazu Tada. Low frequency noise in organic solar cells. In *Noise and Fluctuations (ICNF), 2011 21st International Conference on*, pages 77–79, June 2011.

[55] O. Marinov and M.J. Deen. Flicker noise due to variable range hopping in organic thin-film transistors. In *Noise and Fluctuations (ICNF), 2011 21st International Conference on*, pages 287–290, June 2011.

[56] C. Y. Han, L. X. Qian, C. H. Leung, C. M. Che, and P. T. Lai. A low-frequency noise model with carrier generation-recombination process for pentacene organic thin-film transistor. *Journal of Applied Physics*, 114(4):–, 2013.

[57] K.Y. Choo, S.V. Muniandy, C.L. Chua, and K.L. Woon. Scaling behaviors of transient noise current in organic field-effect transistors. *Organic Electronics*, 13(8):1370–1376, August 2012.

[58] Hongki Kang, Lakshmi Jagannathan, and Vivek Subramanian. Measurement, analysis, and modeling of 1/f noise in pentacene thin film transistors. *Applied Physics Letters*, 99(6):–, 2011.

[59] Yong Xu, Takeo Minari, Kazuhito Tsukagoshi, Jan Chroboczek, Francis Balestra, and Gerard Ghibaudo. Origin of low-frequency noise in pentacene field-effect transistors. *Solid-State Electronics*, 61(1):106 – 110, 2011.

[60] Yong Xu, Chuan Liu, W. Scheideler, Songlin Li, Wenwu Li, Yen-Fu Lin, F. Balestra, G. Ghibaudo, and K. Tsukagoshi. Understanding thickness-dependent charge transport in pentacene transistors by low-frequency noise. *Electron Device Letters, IEEE*, 34(10):1298–1300, Oct 2013.

[61] Lin Ke, S. Bin Dolmanan, Chellappan Vijila, Soo Jin Chua, Ye Hua Han, and Ting Mei. Investigation of the device degradation mechanism in pentacene-based thin-film transistors using low-frequency-noise spectroscopy. *Electron Devices, IEEE Transactions on*, 57(2):385–390, Feb 2010.

[62] Lin Ke, Surani Bin Dolmanan, Lu Shen, Chellappan Vijila, Soo Jin Chua, Rui-Qi Png, Perq-Jon Chia, Lay-Lay Chua, and Peter K.-H. Ho. Low frequency noise analysis on organic thin film transistors. *Journal of Applied Physics*, 104(12):–, 2008.

[63] C. Bonavolont, C. Albonetti, M. Barra, and M. Valentino. Electrical mobility in organic thin-film transistors determined by noise spectroscopy. *Journal of Applied Physics*, 110(9):–, 2011.

[64] O. Marinov, M.J. Deen, and B. Iniguez. Charge transport in organic and polymer thin-film transistors: recent issues. *Circuits, Devices and Systems, IEE Proceedings* -, 152(3):189–209, June 2005.

[65] L. K. J. Vandamme, R. Feyaerts, Gy. Trefn, and C. Detcheverry. 1/f noise in pentacene and poly-thienylene vinylene thin film transistors. *Journal of Applied Physics*, 91(2):719–723, 2002.

[66] M.J. Deen, O. Marinov, S. Holdcroft, and W. Woods. Low-frequency noise in polymer transistors. *Electron Devices, IEEE Transactions on*, 48(8):1688–1695, Aug 2001.

[67] P. V. Necliudov, S. L. Rumyantsev, M. S. Shur, D. J. Gundlach, and T. N. Jackson. 1/f noise in pentacene organic thin film transistors. *Journal of Applied Physics*, 88(9):5395–5399, 2000.

[68] Hongki Kang and Vivek Subramanian. Measurement and analysis of 1/f noise under switched bias in organic thin film transistors. *Applied Physics Letters*, 104(2):–, 2014.

[69] Zhang Jia, I. Meric, Kenneth L. Shepard, and I. Kymissis. Doping and illumination dependence of 1/f noise in pentacene thin-film transistors. *Electron Device Letters, IEEE*, 31(9):1050–1052, Sept 2010.

[70] David Burdeaux, Paul Townsend, Joseph Carr, and Philip Garrou. Benzocyclobutene (bcb) dielectrics for the fabrication of high density, thin film multichip modules. *Journal of Electronic Materials*, 19(12):1357–1366, 1990.

[71] Letian Dou, Jingbi You, Jun Yang, Chun-Chao Chen, Youjun He, Seiichiro Murase, Tom Moriarty, Keith Emery, Gang Li, and Yang Yang. Tandem polymer solar cells featuring a spectrally matched low-bandgap polymer. *Nat Photon*, 6(3):180–185, March 2012.

[72] H. Achour, B. Cretu, J.-M. Routoure, R. Carin, R. Talmat, A. Benfdila, E. Simoen, and C. Claeys. In depth static and low-frequency noise characterization of n-channel finfets on {SOI} substrates at cryogenic temperature. *Solid-State Electronics*, 98(0):12 – 19, 2014. Selected Papers from {ULIS} 2013 Conference.

[73] J. Cayssol, B. Huard, and D. Goldhaber-Gordon. Contact resistance and shot noise in graphene transistors. *Phys. Rev. B*, 79:075428, Feb 2009.

[74] Hsien-Chin Chiu, Chia-Hsuan Wu, Che-Kai Lin, and Feng-Tso Chien. Investigation of impact ionization and flicker noise properties in indium aluminum arsenide/indium gallinum arsenide metamorphic high electron mobility transistors with various work function-gate metals. *Materials Science in Semiconductor Processing*, 30(0):41 – 47, 2015.

[75] John H. Scofield. A.c. method for measuring low-frequency resistance fluctuation spectra. *Review of Scientific Instruments*, 58(6):985–993, 1987.

[76] Aveek Bid, Achyut Bora, and A K Raychaudhuri. 1/ f noise in nanowires. *Nanotechnology*, 17(1):152, 2006.

[77] Lay-Lay Chua, Jana Zaumseil, Jui-Fen Chang, Eric C.-W. Ou, Peter K.-H. Ho, Henning Sirringhaus, and Richard H. Friend. General observation of n-type field-effect behaviour in organic semiconductors. *Nature*, 434(7030):194–199, March 2005.

[78] Satyaprasad P. Senanayak, A. Z. Ashar, Catherine Kanimozhi, Satish Patil, and K. S. Narayan. Room-temperature bandlike transport and hall effect in a high-mobility ambipolar polymer. *Phys. Rev. B*, 91:115302, Mar 2015.

[79] Gilles Horowitz, Riadh Hajlaoui, Habib Bouchriha, Ramzi Bourguiga, and Mohcen Hajlaoui. The concept of "threshold voltage" in organic field-effect transistors. *Advanced Materials*, 10(12):923–927, 1998.

[80] Y. Xu, T. Minari, K. Tsukagoshi, R. Gwoziecki, R. Coppard, F. Balestra, J. A. Chroboczek, and G. Ghibaudo. Extraction of low-frequency noise in contact resistance of organic field-effect transistors. *Applied Physics Letters*, 97(3):–, 2010.

[81] M. Koyama, M. Casse, R. Coquand, S. Barraud, G. Ghibaudo, H. Iwai, and G. Reimbold. Study of low-frequency noise in soi tri-gate silicon nanowire mosfets. *ICNF*, pages 1–4, June 2013.

[82] RI Badran, C Main, and S Reynolds. Analysis and modelling of generation–recombination noise in amorphous semiconductors. *Thin solid films*, 427(1):133–136, 2003.